© 2014. Published by The Company of Biologists Ltd | Journal of Cell Science (2014) 127, 2709–2722 doi:10.1242/jcs.143446

RESEARCH ARTICLE

Arl13b and the non-muscle myosin heavy chain IIA are required for circular dorsal ruffle formation and cell migration

Cristina Casalou, Cecília Seixas, Ana Portelinha, Petra Pintado, Mafalda Barros, José S. Ramalho, Susana S. Lopes and Duarte C. Barral*

ABSTRACT

The Arf-like protein Arl13b has been implicated in ciliogenesis and Sonic hedgehog signaling. Furthermore, we have previously shown that it regulates endocytic recycling traffic and interacts with actin. Herein, we report that the non-muscle myosin heavy chain IIA, also known as Myh9, is an Arl13b effector. Moreover, we found that both proteins localized to circular dorsal ruffles (CDRs) induced by platelet-derived growth factor stimulation and are required for their formation. CDRs are ring-shaped actin-dependent structures formed on the dorsal cell surface and are involved in diverse processes, such as macropinocytosis, integrin recycling, internalization of receptor tyrosine kinases and cell migration. We found that Arl13b or Myh9 silencing impaired cell migration, suggesting that Arl13b is required for this function through the interaction with Myh9. Moreover, Arl13b silencing impaired neural crest cell migration in zebrafish embryos. Furthermore, we showed that Arl13b is required for the formation of CDRs in migrating cells. Thus, our results indicate a new role for Arl13b in actin cytoskeleton remodeling through the interaction with Myh9, by driving the formation of CDRs necessary for cell migration.

KEY WORDS: Arl13b, Myosin heavy chain IIA, Myh9, Circular dorsal ruffle, Small G protein, Actin cytoskeleton, Platelet-derived growth factor signaling, Wound healing

INTRODUCTION

Cell migration is essential during development and wound healing, and has been implicated in human diseases, such as atherosclerosis and cancer (Ridley et al., 2003, Raftopoulou and Hall, 2004). At the intracellular level, cell migration has been shown to be regulated by polarized vesicle trafficking and recycling of internalized proteins to the leading edge of migrating cells (Fletcher and Rappoport, 2010; Ulrich and Heisenberg, 2009). During this process, extracellular growth factors activate receptor tyrosine kinase (RTK)-dependent signaling, leading to extensive actin cytoskeleton remodeling and to the formation of unique specialized structures, such as circular dorsal ruffles (CDRs), lamellipodia and filopodia. CDRs are highly dynamic ring-shaped structures that are rich in filamentous actin (F-actin), and form on the dorsal surface of epithelial cells and fibroblasts in response to stimulation with growth factors, such as platelet-derived growth factor (PDGF) and epidermal growth factor (EGF) (Hoon et al., 2012). Moreover, CDRs have been implicated in macropinocytosis (Dowrick et al., 1993), recycling of integrins (Gu et al., 2011), rapid actin cytoskeleton remodeling during cell migration (Buccione et al., 2004), and in the internalization and sequestration of a number of RTKs, leading to their downregulation (Orth and McNiven, 2006).

Members of the Ras superfamily of small G proteins have been shown to play key roles in CDR formation. For instance, Rac1 and Rab5 have been found to be necessary for CDR formation by controlling intracellular trafficking through early endosomes (Lanzetti et al., 2004; Palamidessi et al., 2008). Small G proteins can cycle between inactive GDP-bound and active GTP-bound conformations. When in their GTP-bound form, they recruit effector proteins that mediate vesicle budding from donor organelles, vesicle transport along microtubules or actin filaments, and tethering and fusion of vesicles to acceptor compartments. Therefore, they control protein secretion, endocytosis, recycling and degradation, among other functions, and are widely recognized as essential regulators of intracellular trafficking.

ADP-ribosylation-factor-like (Arl) proteins belong to the Arf family of small G proteins and are thought to regulate vesicle tethering to acceptor membrane compartments, as well as cytoskeleton organization (Donaldson and Jackson, 2011). However, their functions are still largely unknown and, for most of them, there are no known effectors. Interestingly, several Arl proteins, namely Arl3, Arl6 and Arl13b, have been associated with the primary cilium, a mechanosensory organelle involved in signal transduction. *Arl13b* was identified as one causal locus for the ciliopathy Joubert syndrome, an autosomal recessive disorder characterized by congenital cerebellar ataxia, hypotonia, oculomotor apraxia, mental retardation, cystic kidneys and polydactyly (Cantagrel et al., 2008). *Arl13b*^{hnn} mutant mice [also known as *hennin* mice (*hnn*)] mimic the phenotype of Joubert syndrome patients, and show coupled defects in cilia structure and Sonic hedgehog (Shh) signaling (Caspary et al., 2007; Larkins et al., 2011, Horner and Caspary, 2011).

Recently, we demonstrated that Arl13b regulates endocytic recycling traffic (Barral et al., 2012). Additionally, we have observed that Arl13b colocalizes with the actin cytoskeleton and that it interacts with actin. Herein, we describe a new role for Arl13b in the formation of CDRs. Moreover, we found that Arl13b is required for cell migration, both *in vitro* and *in vivo* and that it is necessary for CDR formation in migrating cells. Furthermore, we identified the motor protein non-muscle myosin heavy chain IIA, also known as Myh9, as an Arl13b effector. Myh9 is one of the three isoforms of the non-muscle myosin II

CEDOC, Faculdade de Ciências Médicas, Universidade Nova de Lisboa, 1169-056 Lisboa, Portugal.

*Author for correspondence (duarte.barral@fcm.unl.pt)

Received 26 September 2013; Accepted 18 March 2014

Journal of Cell Science

Journal of Cell Science (2014) 127, 2709–2722 doi:10.1242/jcs.143446

heavy chain found in humans and has been implicated in the generation of cell polarity, cell motility, directional cell migration and cell–cell adhesion (Conti and Adelstein, 2008; Vicente-Manzanares et al., 2009). In addition, there is evidence that Myh9 is involved in the docking and fusion events of the secretory pathway that take place in the apical domain, below the plasma membrane (Bond et al., 2011). Interestingly, we found that Myh9 is also necessary for the formation of CDRs induced by PDGF stimulation and for the interaction between Arl13b and actin. Thus, our findings suggest that the mechanism by which Arl13b and Myh9 regulate actin remodeling is by driving the formation of CDRs that are required for cell migration.

RESULTS

Arl13b localizes to circular dorsal ruffles

We have previously found that Arl13b interacts with actin and colocalizes with actin filaments and cortical actin (Barral et al., 2012). We extended these results and found that Arl13b localizes in actin-rich peripheral regions that are consistent with lamellipodia and filopodia (Fig. 1A). We also analyzed whether Arl13b was present in other actin-dependent structures. Strikingly, when NIH-3T3 cells expressing wild-type Arl13b tagged with EGFP (Arl13b-wt–EGFP) were treated with the growth factor PDGF-BB (the PDGF homodimer comprising two PDGFB chains) for 20 minutes to induce CDR formation, we found that Arl13b localized to

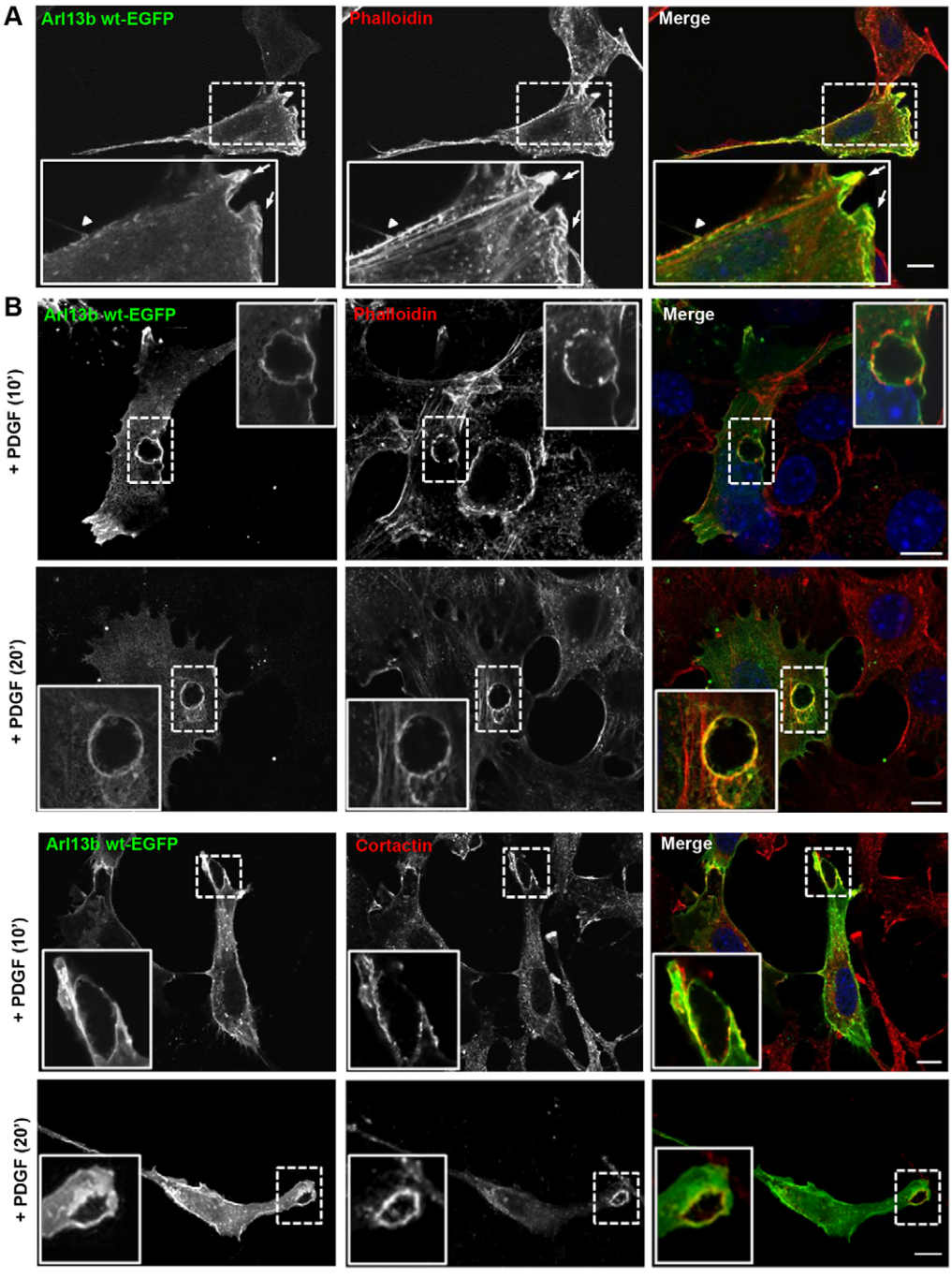

Fig. 1. Colocalization of Arl13b with actin-rich structures. (A) NIH-3T3 cells expressing Arl13b-wt–EGFP (Arl13b wt-EGFP) were fixed and stained with Alexa-Fluor-568-conjugated phalloidin. At the cell periphery, Arl13b localizes in actin-rich structures that are consistent with lamellipodia (arrows) and filopodia (arrowhead). (B) NIH-3T3 cells expressing Arl13b-wt–EGFP were stimulated with PDGF-BB (30 ng/ml) for the indicated times, fixed and stained with Alexa-Fluor-568-conjugated phalloidin to label actin or with mouse monoclonal anti-cortactin antibody. Enlarged views of the indicated sections are shown in the insets. Scale bars: 10 μm.

Journal of Cell Science (2014) 127, 2709–2722 doi:10.1242/jcs.143446

these structures, identified by the presence of both F-actin and the specific CDR marker cortactin (Ammer and Weed, 2008) (Fig. 1B). Moreover, when human primary fibroblasts were transduced with lentiviruses encoding Arl13b-wt–EGFP, upon PDGF stimulation, the protein was readily identified in CDRs labeled by phalloidin or cortactin, suggesting that this localization is not exclusive to transformed cell lines (supplementary material Fig. S1A). Furthermore, to study Arl13b localization during CDR formation, F-actin and Arl13b were monitored by time-lapse microscopy in PDGF-stimulated NIH-3T3 cells coexpressing Arl13b-wt–EGFP and Lifeact-ruby, which binds F-actin. We observed the formation of a circular structure, identified as a CDR because it is enriched in F-actin, within the first 20 minutes of PDGF stimulation (supplementary material Fig. S1B; Movie 1). This suggests that the localization of Arl13b in CDRs is not an artifact of fixation and occurs in live cells. Taken together, these results show that Arl13b becomes rapidly concentrated in CDRs in response to growth factor stimulation.

Arl13b is required for circular dorsal ruffle formation

Given that Arl13b interacts with actin and localizes to CDRs, we asked whether it can regulate their formation. For this, we used two distinct short hairpin RNAs (shRNAs) targeting Arl13b, to achieve between 50 and 88% reduction in Arl13b protein levels, as determined by immunoblotting (supplementary material Fig. S2A). CDRs were present in ~49% of cells transduced with shRNA control and stimulated with PDGF-BB for 10 minutes, and in 47% of control mock-transfected cells, whereas only ~19.5% of the Arl13b-silenced cells formed CDRs, which were also noticeably smaller (Fig. 2A,B). Furthermore, we quantified CDR formation in Arl13b-deficient mouse embryonic fibroblasts (MEFs) over a timecourse and observed that the formation of CDRs was impaired in *Arl13b*^{hnn} MEFs throughout the 30 minutes of PDGF stimulation, as compared to wild-type MEFs (supplementary material Fig. S2B,C). Finally, we confirmed that in human primary fibroblasts, Arl13b silencing also impaired CDR formation (supplementary material Fig. S2D). Importantly, this defect in CDR formation was rescued by exogenous expression of Arl13b-wt–EGFP (Fig. 2B), showing that the impairment in CDR formation upon Arl13b silencing is not an off-target effect. Arl13b differs substantially from other Arls because it contains a long C-terminal domain of largely unknown function. We have previously found that Arl13b 1–193 truncation mutant, which does not contain the C-terminal region of Arl13b, is unable to colocalize with the actin cytoskeleton (Barral et al., 2012). As a further control for the specificity of the impairment of CDR formation in Arl13b-depleted cells, we expressed exogenous EGFP-tagged Arl13b 1–193 (Arl13b-1–193–EGFP) in cells where the expression of Arl13b was silenced. We observed that unlike Arl13b-wt–EGFP, Arl13b-1–193–EGFP was not capable of rescuing CDR formation after Arl13b silencing, further confirming the specificity of the rescue (Fig. 2B). Furthermore, a mock control of the transfection confirmed the specificity of the rescue obtained by exogenous expression of Arl13b-wt–EGFP. By contrast, cells overexpressing Arl13b-wt–EGFP displayed an ~2.5-fold increase in CDR formation upon PDGF stimulation for 20 minutes, when compared to cells expressing EGFP or Arl13b-1–193–EGFP (Fig. 2C). Taken together, these results strongly suggest that Arl13b is required for the formation of PDGF-induced CDRs.

Arl13b associates with macropinosomes and with early and recycling endosomes

CDRs have been implicated in macropinocytosis, a regulated form of endocytosis that mediates the non-selective uptake of fluid-phase cargo (Swanson, 2008; Kerr and Teasdale, 2009). This process can be monitored by following fluid-phase markers, such as dextran (Kerr and Teasdale, 2009). Given that Arl13b is necessary for CDR formation, we investigated whether Arl13b-labeled CDRs matured into macropinosomes. To this end, NIH-3T3 cells expressing Arl13b-wt–EGFP were incubated with dextran in the presence of PDGF, and dextran uptake was monitored by confocal microscopy over a timecourse. After 5 minutes of PDGF stimulation, we observed Arl13b in circular structures that were labeled by F-actin but did not contain dextran (Fig. 3A). Therefore, they can be identified as CDRs, which are open to the extracellular milieu and are not able to retain fluid-phase markers. Interestingly, after 10 minutes of PDGF stimulation, cells expressing Arl13b-wt–EGFP showed dextran accumulation in structures that contained Arl13b but were negative for F-actin (Fig. 3A). These can be identified as macropinosomes, which are intracellular structures that retain fluid-phase markers and are devoid of F-actin. Thus, these observations suggest that after being recruited to CDRs, Arl13b is incorporated into macropinosomes.

Next, we sought to assess the localization of Arl13b after a longer incubation with PDGF, because after macropinosome disassembly, cargo that has been taken up through CDRs, such as integrins, traffics through early and recycling endosomes (Gu et al., 2011). Interestingly, we observed that after 30 minutes of PDGF stimulation, Arl13b partially colocalized with early endosome markers (EEA1 and Rab5a), as well as with a recycling endosome marker (transferrin), in small vesicles dispersed throughout the cytoplasm (Fig. 3B–D). This supports our previous studies, where we found a role for Arl13b in the recycling pathway (Barral et al., 2012). Taken together, this data suggests that Arl13b is internalized upon growth factor stimulation in CDRs and traffics through early and recycling endosomes.

Arl13b is required for *in vitro* and *in vivo* cell migration

In order to investigate whether Arl13b is associated with CDR-dependent functions, we examined whether Arl13b is required for cell migration. For this, we monitored cell migration in two different ways, namely by using scratch 'wound healing' and transwell migration assays. In the former, a monolayer of cells was scratched with a pipette tip. The migration of cells to close the 'wound' was assessed after 16 hours by measuring the area free of cells. Strikingly, Arl13b silencing resulted in a significant delay (~50%) in PDGF-dependent wound closure in NIH-3T3 cells (Fig. 4A,B). Next, we confirmed that Arl13b deficiency in *Arl13b*^{hnn} MEFs also resulted in delayed wound closure (supplementary material Fig. S3A,B). Similarly, we observed that Arl13b silencing in HeLa cells led to impairment in wound closure (supplementary material Fig. S3C), suggesting that Arl13b requirement for cell migration is general and conserved. Moreover, given that HeLa cells do not possess cilia (Alieva et al., 1999), this function is presumably independent of the primary cilium, where Arl13b has a known role. Conversely, when Arl13b-wt–EGFP was overexpressed in NIH-3T3 or HeLa cells, an increase in the percentage of wound closure was observed when compared with cells overexpressing Arl13b-1–193–EGFP, EGFP or non-transfected cells (Fig. 4C; supplementary material Fig. S3D). Furthermore, cell migration

Journal of Cell Science (2014) 127, 2709–2722 doi:10.1242/jcs.143446

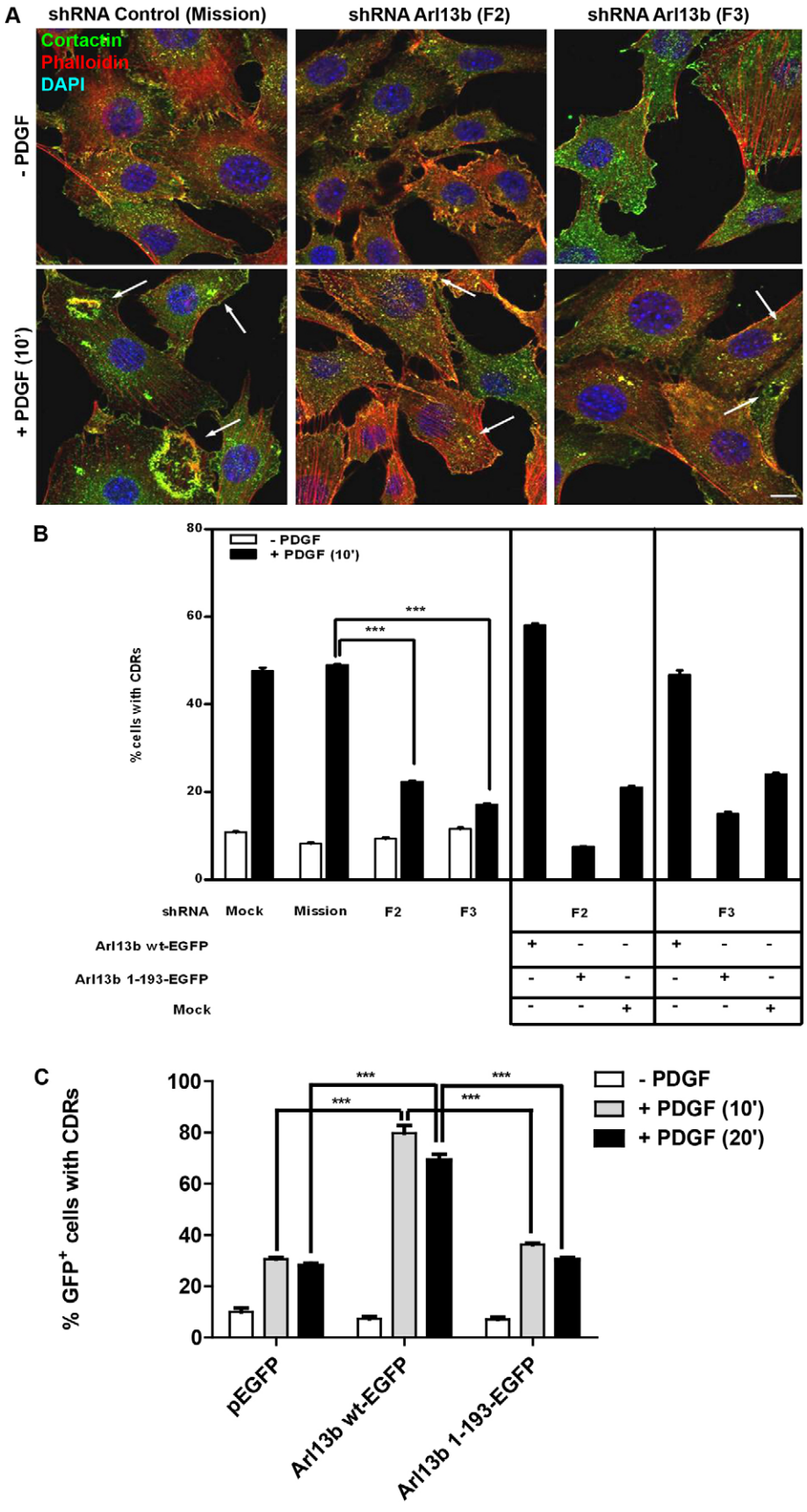

Fig. 2. Arl13b is required for CDR formation. NIH-3T3 cells were transduced with Arl13b shRNAs (F2 and F3), control shRNA (Mission) or no shRNA (Mock), followed by starvation and treatment with PDGF-BB for 10 minutes (30 ng/ml). (A) NIH-3T3 cells transduced with either control or Arl13b shRNAs were stimulated with PDGF-BB for 10 minutes and stained with Alexa-Fluor-568-conjugated phalloidin and anti-cortactin antibody to identify CDRs. DAPI was used to stain nuclei. Arrows indicate CDRs. Scale bar: 10 μm. (B) Quantification of CDRs in control and Arl13b-silenced cells. Rescue experiments were performed by transfection of Arl13b-wt–EGFP (Arl13b wt-EGFP) or Arl13b-1–193–EGFP (Arl13b 1-193-EGFP) constructs. A control of the transfection (Mock) was performed in cells previously transduced with shRNA for Arl13b (F2 and F3). Results are mean±s.d. of three independent experiments; 125–150 cells were counted per experiment. (C) Quantification of PDGF-induced CDR formation for the indicated times in cells transiently transfected with Arl13b-wt–EGFP, Arl13b-1–193–EGFP or EGFP, used as a negative control. Results are mean±s.d. of four independent experiments, >200 cells counted per experiment. ***$P<0.001$, two-way ANOVA.

Journal of Cell Science (2014) 127, 2709–2722 doi:10.1242/jcs.143446

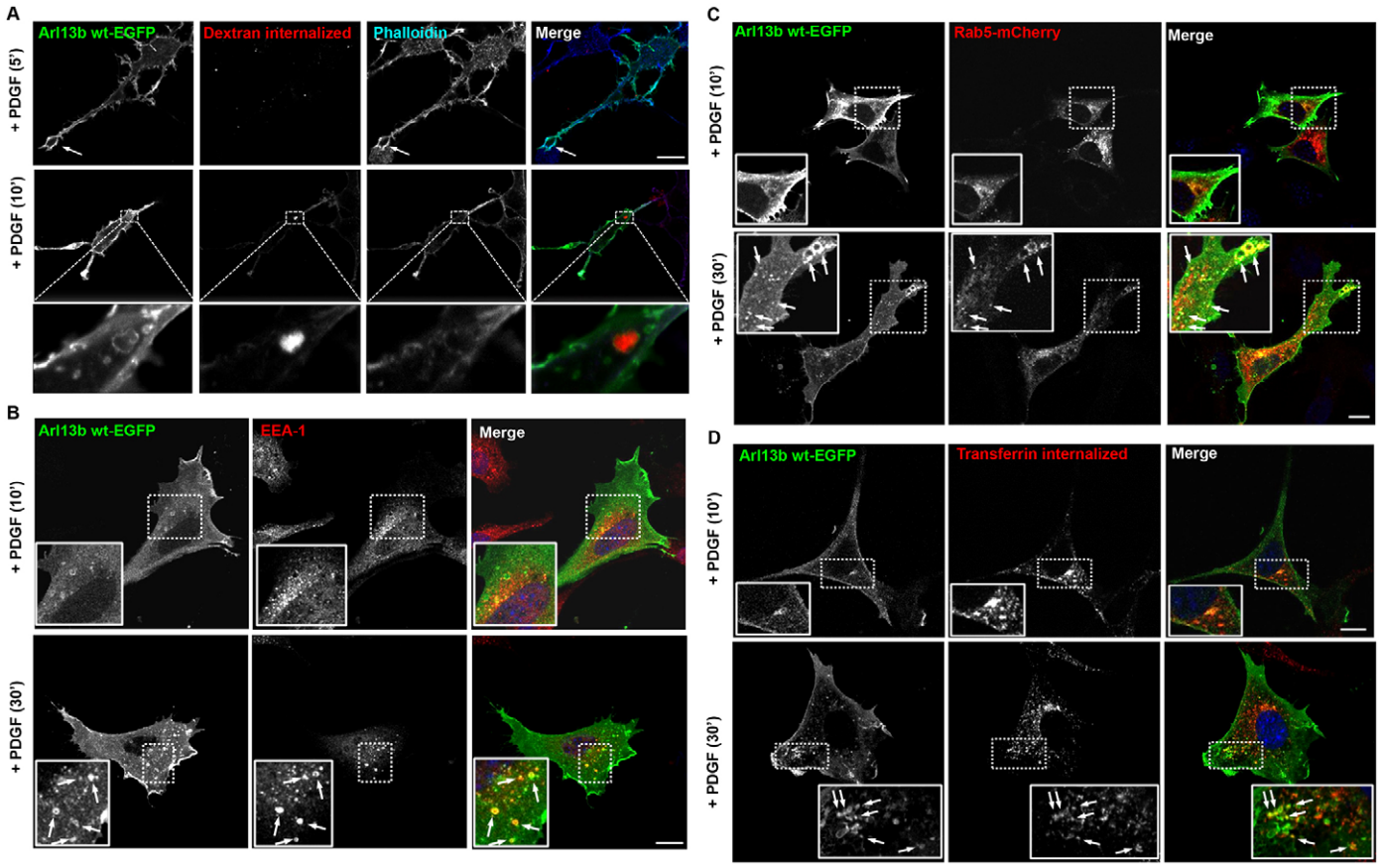

Fig. 3. Arl13b localizes to macropinosomes and colocalizes with early and recycling endosome markers. (A) The fluid-phase marker dextran, conjugated to Alexa Fluor 546 (0.3 mg/ml), was added to the medium of NIH-3T3 cells expressing Arl13b-wt–EGFP (Arl13b wt-EGFP) for 10 minutes and stimulated with PDGF-BB (30 ng/ml) for 5 or 10 minutes. Cells were fixed and stained with Alexa-Fluor-635-conjugated phalloidin for 30 minutes. Arrows point to CDRs; the images in the lower panels are enlarged views of areas indicated by the boxes and show a macropinosome. (B,C) NIH-3T3 cells expressing Arl13b-wt–EGFP and stained with anti-EEA1 antibody (B) or co-expressing Arl13b-wt–EGFP and Rab5a–mCherry (C) were stimulated with PDGF-BB (30 ng/ml) for 10 or 30 minutes and then fixed. (D) NIH-3T3 cells expressing Arl13b-EGFP were incubated with Alexa-Fluor-546-conjugated transferrin (10 μg/ml) for 30 minutes after 1 hour of serum-starvation, and then were stimulated with PDGF (for 10 or 30 minutes) and fixed. Arrows indicate Arl13b in early and recycling endosomes. Scale bars: 10 μm.

was assessed using a modified Boyden chamber transwell assay. Consistent with the scratch wound healing assays, this approach revealed that Arl13b-silenced cells were defective in PDGF-induced cell migration (Fig. 4D,E). Hence, these results show that Arl13b is required for cell migration, as measured by wound healing and transwell assays.

Interestingly, we observed that Arl13b was recruited to the leading edge of cells at the forefront of closing wounds, where it colocalizes with the actin cytoskeleton (supplementary material Fig. S4A). Moreover, CDRs have been implicated in the transition from static to motile cell states (Gu et al., 2011; Sero et al., 2011). Therefore, in order to investigate whether Arl13b-deficient cells cannot migrate properly owing to deficient CDR formation, immunofluorescence analysis was carried out on migrating cells in the wound healing model. For this, NIH-3T3 cell monolayers were fixed 4 hours after scratching, in the presence of PDGF. Typical CDRs, identified by the presence of both phalloidin and cortactin, were observed in ~50% of shRNA control cells lining the edge of the closing wounds, showing that migrating cells possess CDRs. However, in Arl13b-silenced cells, only ~15% of the cells lining the wound edges formed CDRs (Fig. 4F,G). Importantly, Arl13b silencing efficiency was confirmed by immunoblotting (supplementary material Fig. S4B). Taken together, these results suggest that the observed defects in cell migration in cells depleted of Arl13b can be associated with the significant decrease in CDR formation in cells that are migrating into closing wounds.

Finally, we assessed the Arl13b requirement for cell migration in a well-established *in vivo* model. For this, we used the *sox10* gene, which is expressed during neural crest cell migration from the neural tube into the somite region in zebrafish embryos (Dutton et al., 2001). At 24 hours post-fertilization (hpf), migratory neural crest cells, labeled by *sox10*, gradually migrated from the neural tube into the trunk of wild-type embryos (Fig. 4H). However, when zebrafish embryos were treated with a morpholino antisense oligonucleotide to temporarily silence Arl13b expression, there was a significant delay in the onset of migration of neural crest cells expressing *sox10* when compared to stage-matched siblings (Fig. 4H). Importantly, this defect in neural crest cell migration could be rescued when Arl13b morpholino was injected into Arl13b transgenic zebrafish embryos that overexpress mouse Arl13b, which is not targeted by the morpholino (Borovina et al., 2010) (Fig. 4H). Taken together, these results show that Arl13b is required for cell migration both *in vitro* and *in vivo*, probably through the formation of CDRs at sites of migration.

Journal of Cell Science (2014) 127, 2709–2722 doi:10.1242/jcs.143446

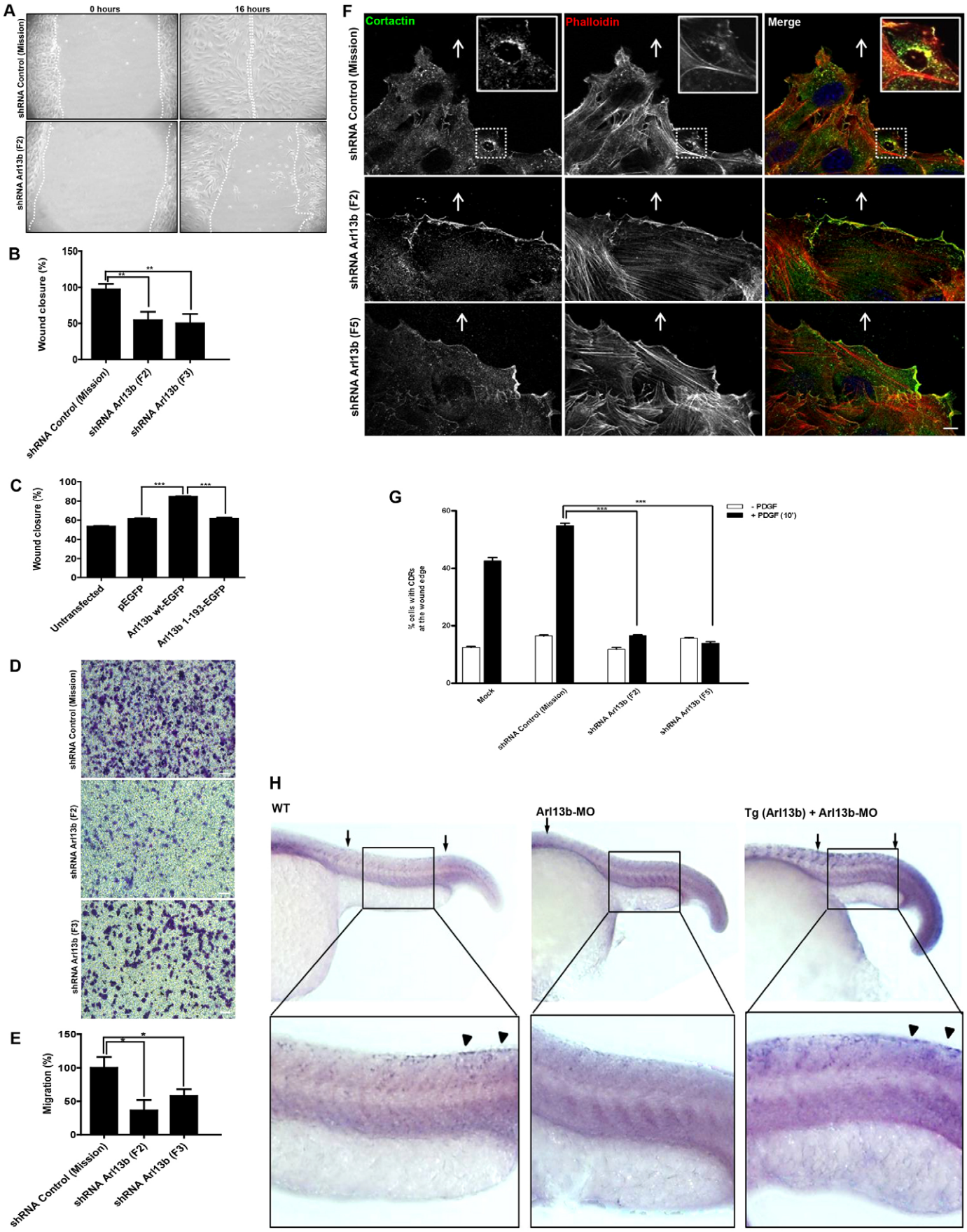

Fig. 4. See next page for legend.

Journal of Cell Science (2014) 127, 2709–2722 doi:10.1242/jcs.143446

Fig. 4. Arl13b is required for cell migration. Endogenous Arl13b was silenced by specific shRNAs (F2 and F3) in NIH-3T3 cells. (A) Control or Arl13b-silenced cells grown to confluence were scratched with a pipette tip and stimulated with PDGF to induce cell migration. Representative images taken at 0 and 16 hours post-wounding of control and Arl13b-silenced cells are shown. (B) Quantitative analysis of wound closure (%) after 16 hours was performed as described in Materials and Methods. Results are mean±s.d. of three independent experiments. (C) NIH-3T3 cells expressing Arl13b-wt–EGFP (Arl13b wt-EGFP), Arl13b-1–193–EGFP (Arl13b 1-193-EGFP) or EGFP for 24 hours were allowed to form a monolayer and then scratched. Quantitative analysis of wound closure (%) was performed 16 hours after scratching. Results are mean±s.d. of three independent experiments. (D) Arl13b-silenced or control NIH-3T3 cells were added to the upper chamber of 8-μm-pore membranes and allowed to migrate for 6 hours. Representative fields of Crystal-Violet-stained cells that migrated to the lower surface of the membranes are shown for control shRNA (Mission) and Arl13b shRNAs (F2 and F3). Scale bars: 100 μm. (E) Quantification of the transwell migration was performed as described in Materials and Methods. Results are mean±s.d. of three independent experiments. (F) Immunofluorescence analysis of CDR formation at the leading edge of migrating control and Arl13b-silenced cells. After 4 hours of incubation in the presence or absence of PDGF-BB (20 ng/ml), cells were fixed and stained with Alexa-Fluor-568-conjugated phalloidin and anti-cortactin antibody to identify CDRs. DAPI was used to stain nuclei. Arrows indicate wound direction, and insets show CDRs at higher magnification. Scale bar: 10 μm. (G) Quantification of CDRs in control (Mock and shRNA Mission) and Arl13b-silenced cells (shRNAs F2 and F5) at the edge of closing wounds. Results are mean±s.d. of three independent experiments. (H) Neural crest cell migration in Arl13b morpholino (MO)-injected zebrafish embryos. At 24 hours post fertilization, zebrafish embryos injected with Arl13b-MO and hybridized with *sox10* probe, revealed that trunk neural crest cells failed to migrate ($n=17$), when compared with uninjected wild-type siblings (WT, $n=18$). Arrows indicate the region where neural crest cell migration occurred from anterior to posterior somites. Rescue was performed by injection of Arl13b-MO in a zebrafish transgenic line [Tg (Arl13b)], which expresses mouse Arl13b–GFP (which is not targeted by the morpholino) in addition to the endogenous zebrafish Arl13b ($n=16$). Arrowheads indicate neural crest cells at the posterior somites. *$P<0.05$; **$P<0.005$ (B,E, Student's *t*-test); ***$P<0.001$ (C,G, two-way ANOVA).

Non-muscle myosin heavy chain IIA is an Arl13b effector

To determine the molecular mechanism by which Arl13b interacts with actin and mediates CDR formation, we attempted to identify Arl13b-binding partners. Moreover, by co-immunoprecipitation of cell extracts loaded with a non-hydrolyzable analog of GTP, GTPγS, we specifically attempted to identify Arl13b effectors that bind to the active form of the protein. Interestingly, we were able to detect a band of ~230 kDa in one-dimensional SDS-PAGE that was absent in the control (IgG) and GDP-loaded lanes (Fig. 5A). After mass spectrometry of tryptic peptides, this band was identified as the non-muscle heavy chain myosin IIA, which is also known as Myh9. This myosin is a ubiquitously expressed contractile protein that has been implicated in the regulation of cell spreading and directional cell migration in response to several stimuli (Vicente-Manzanares et al., 2009; Conti and Adelstein, 2008). We confirmed the interaction between Myh9 and Arl13b by co-immunoprecipitation using an anti-Arl13b antibody followed by detection of Myh9 in NIH-3T3 cell extracts by immunoblotting (Fig. 5B). In agreement with the proteomics approach, a band with the expected size of about 230 kDa was observed when the co-immunoprecipitation was performed in the presence of GTPγS, but not in the presence of GDP or in control reactions where an isotype control antibody was used (Fig. 5B). This result shows that Myh9 interacts with Arl13b only when Arl13b is in its active state, that is, Myh9 is a bona fide Arl13b effector. Importantly, when a similar strategy was employed in Arl13b-depleted cells, namely *Arl13b*^{hnn} MEFs, the interaction between Arl13b and Myh9 could not be detected (Fig. 5C), showing the specificity of the binding.

We have previously shown that Arl13b co-immunoprecipitates with β-actin (Barral et al., 2012). Interestingly, we now observed that Arl13b interacts preferentially with β-actin when is in its active or GTP-bound form, with a slight but significant increase in binding in response to PDGF (supplementary material Fig. S4C). Finally, to test whether Myh9 is required for the interaction between Arl13b and actin, we studied the effect of Myh9 silencing on this interaction. Strikingly, we observed that in NIH-3T3 cells silenced for Myh9 (Fig. 5E), the interaction of Arl13b with β-actin was abolished (Fig. 5D). Thus, these data strongly suggest that Myh9 binds to Arl13b in its GTP-bound form and is necessary for the interaction between Arl13b and actin.

Myh9 is required for circular dorsal formation and cell migration

To know if Myh9 colocalizes with Arl13b, we used a polyclonal anti-Myh9 antibody to detect the protein in NIH-3T3 cells. In non-stimulated cells, Myh9 colocalized with actin stress fibers in the cytosol and in lamellipodia at the cell periphery (Fig. 6A). After treatment with PDGF, we observed that Myh9 localized to CDRs, which were decorated by phalloidin and cortactin. Moreover, when NIH-3T3 cells transiently expressing Arl13b-wt–EGFP were stimulated with PDGF and immunostained with anti-Myh9 antibody, we observed a striking colocalization between Arl13b and Myh9 in CDRs (Fig. 6A). Furthermore, in Myh9-silenced cells, CDR formation was impaired upon PDGF stimulation for 20 minutes, suggesting that, similar to Arl13b, Myh9 is required for the formation of CDRs (Fig. 6B and supplementary material Fig. S4D). The specificity of this effect was shown by efficient rescue of the CDR formation impairment through the exogenous expression of Myh9–EGFP, using EGFP as a negative control (Fig. 6B). To determine whether Arl13b-mediated CDR formation requires Myh9, Arl13b-wt–EGFP was transiently expressed in control or Myh9-silenced cells. We found that the striking localization of Arl13b in CDRs observed in control cells was reduced when Myh9 was silenced (Fig. 7A,B), suggesting that the recruitment of Arl13b to CDRs is dependent on Myh9. Moreover, expression of Arl13b-wt–EGFP significantly enhanced PDGF-induced CDR formation in control cells but not in Myh9-silenced cells (Fig. 7C). Taken together, these results suggest that Myh9 is necessary for Arl13b-mediated CDR formation and support our previous observations that Arl13b is specifically localized in CDRs upon PDGF-stimulation. Interestingly, Myh9 has previously been shown to be required for cell migration (Betapudi et al., 2006; Even-Ram et al., 2007). Given that we found that Myh9 is an Arl13b effector, and that Arl13b is required for cell migration, we examined the role of Myh9 in cell migration in response to PDGF stimulation. Transfection of NIH-3T3 cells with small interfering RNA (siRNA) targeting Myh9 reduced the percentage of wound closure by half, when compared with siRNA control, confirming previous studies (Fig. 7D,E). Thus, our data strongly suggests that Arl13b regulates CDR formation through the interaction with Myh9.

DISCUSSION

Arl13b has been described to be involved in ciliogenesis and Shh signaling (Caspary et al., 2007; Larkins et al., 2011). Recently, we also found that Arl13b regulates endocytic recycling traffic and that it associates with the actin cytoskeleton and interacts

Journal of Cell Science (2014) 127, 2709–2722 doi:10.1242/jcs.143446

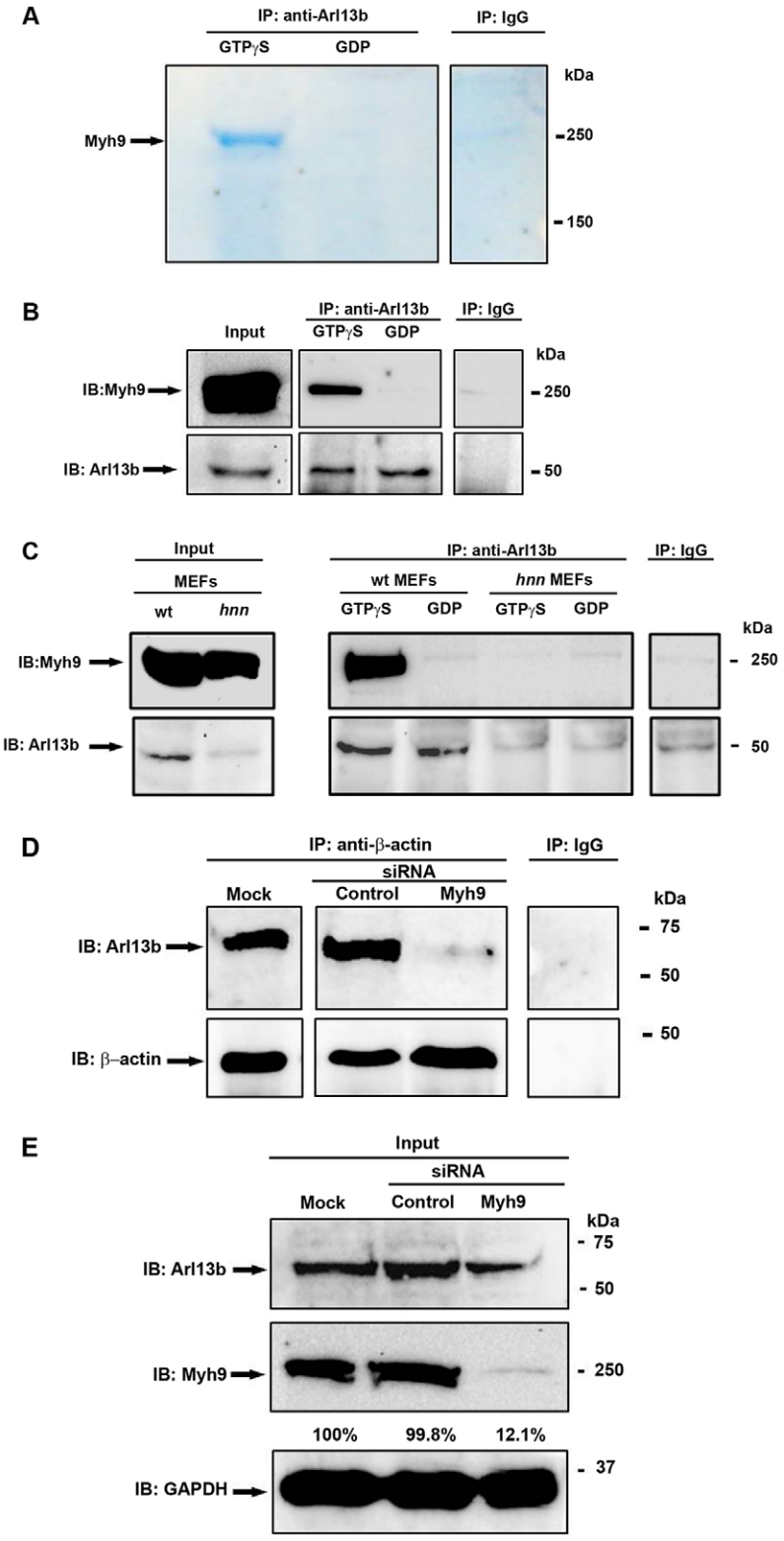

Fig. 5. Myh9 is an Arl13b effector. (A) Lysates from NIH-3T3 cells were immunoprecipitated (IP) with anti-Arl13b antibody in the presence of non-hydrolyzable GTP (GTPγS) or GDP. Rabbit-IgG was used as a negative control. Immunoprecipitated products were analyzed by SDS-PAGE and visualized by Coomassie Brilliant Blue staining. Protein bands were excised and identified by mass spectrometry. (B) Validation of the Myh9–Arl13b interaction by immunoprecipitation of NIH-3T3 lysates with anti-Arl13b antibody or rabbit IgG in the presence of GTPγS or GDP. Immunoprecipitation products were analyzed by immunoblotting (IB) using the indicated antibodies. (C) Total cell lysates obtained from *Arl13b*^{hnn} (*hnn*) and wild-type (wt) MEFs were immunoprecipitated with anti-Arl13b antibody or rabbit IgG in the presence of GTPγS or GDP. The immunoprecipitated products were analyzed by immunoblot with the indicated antibodies. (D,E) NIH-3T3 cell lysates from cells transfected with siRNA control or siRNA targeting Myh9, or that had been mock-transfected, were subjected to immunoprecipitation with anti-β-actin antibody in the presence of GTPγS or with mouse IgG_1 isotype, as a negative control. Immunoprecipitation products were analyzed by immunoblotting using anti-Arl13b antibody. (E) Myh9 silencing was confirmed in the input with anti-Myh9 antibody. Anti-GAPDH antibody was used as a loading control. The percentage of Myh9 expression relative to Mock, determined using ImageJ software, is indicated.

with actin (Barral et al., 2012). Here, we identify a new role for Arl13b in the formation of CDRs and in cell migration. In particular, we found that Arl13b becomes associated with the actin cytoskeleton that encircles CDRs in response to growth factor stimulation, and with the macropinosomes that form after CDR closure. CDRs constitute important platforms for sequestration and internalization of membrane-bound proteins, such as growth factor receptors, and also exert an important role in the fast remodeling of the actin cytoskeleton during cell migration. In recent years, several reports have identified new regulators of CDRs (Hoon et al., 2012). Previous studies have shown that the Rac, Ras and Rab5 small GTPases play a role in the regulation of CDR formation (Palamidessi et al., 2008). In addition, overexpression of Arf GTPase-activating proteins

Journal of Cell Science (2014) 127, 2709–2722 doi:10.1242/jcs.143446

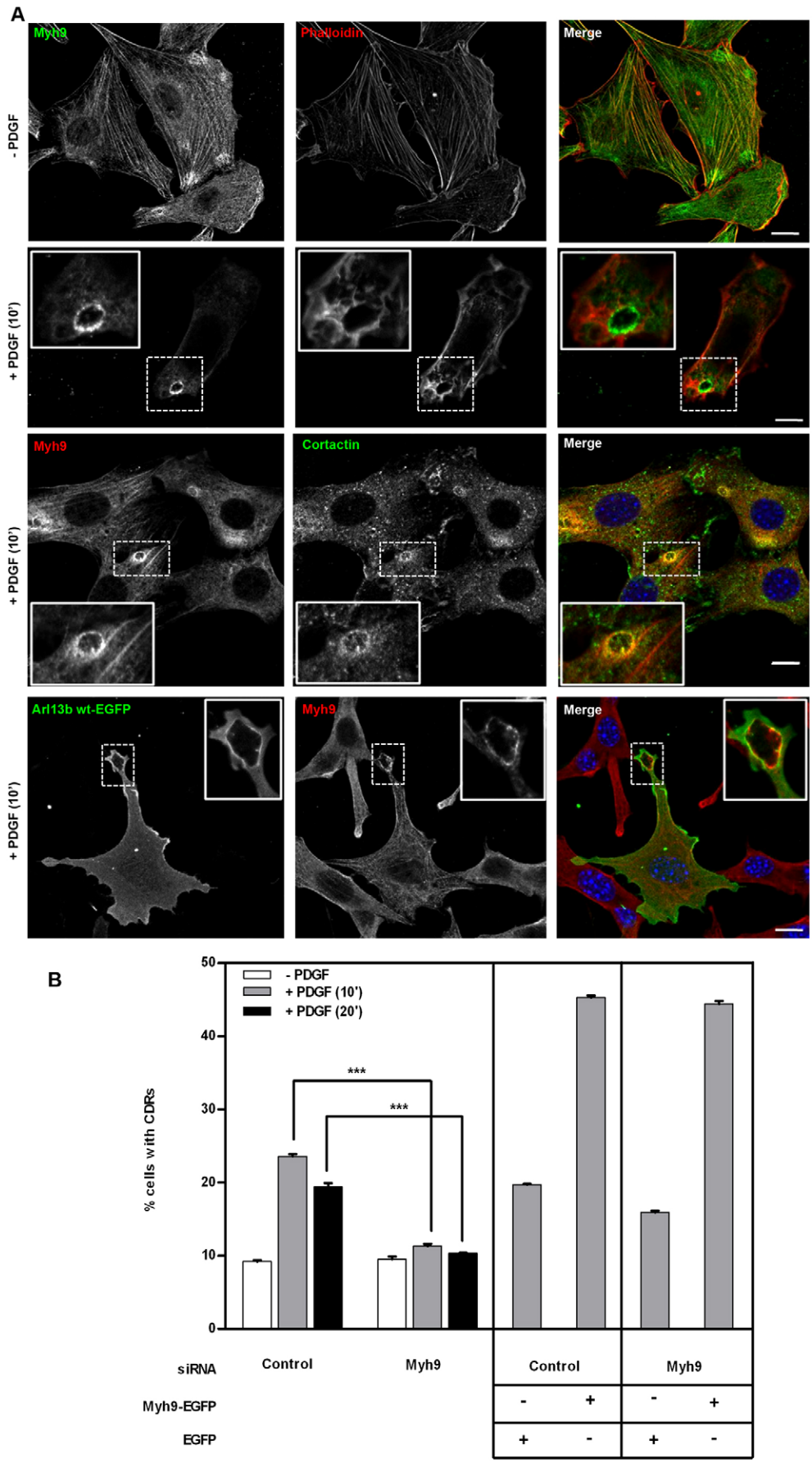

Fig. 6. Myh9 colocalizes with Arl13b in CDRs and is required for CDR formation. (A) NIH-3T3 cells transfected with Arl13b-wt–EGFP (Arl13b wt-EGFP) or not were serum-starved, stimulated with PDGF-BB (30 ng/ml) for 10 minutes, fixed and stained with anti-Myh9 and anti-cortactin antibodies or Alexa-Fluor-568-conjugated phalloidin. Scale bars: 10 μm. (B) Myh9-silenced and control cells were serum-starved and stimulated with PDGF-BB (30 ng/ml) for 10 or 20 minutes, fixed and stained with anti-cortactin antibody and Alexa-Fluor-568-conjugated phalloidin to identify CDRs. Rescue experiments were performed on control cells and cells silenced for Myh9, by transiently expressing Myh9–EGFP or EGFP. Results are mean±s.d. of three independent experiments; >150 cells counted per experiment in each condition. ***$P<0.001$, two-way ANOVA.

Journal of Cell Science (2014) 127, 2709–2722 doi:10.1242/jcs.143446

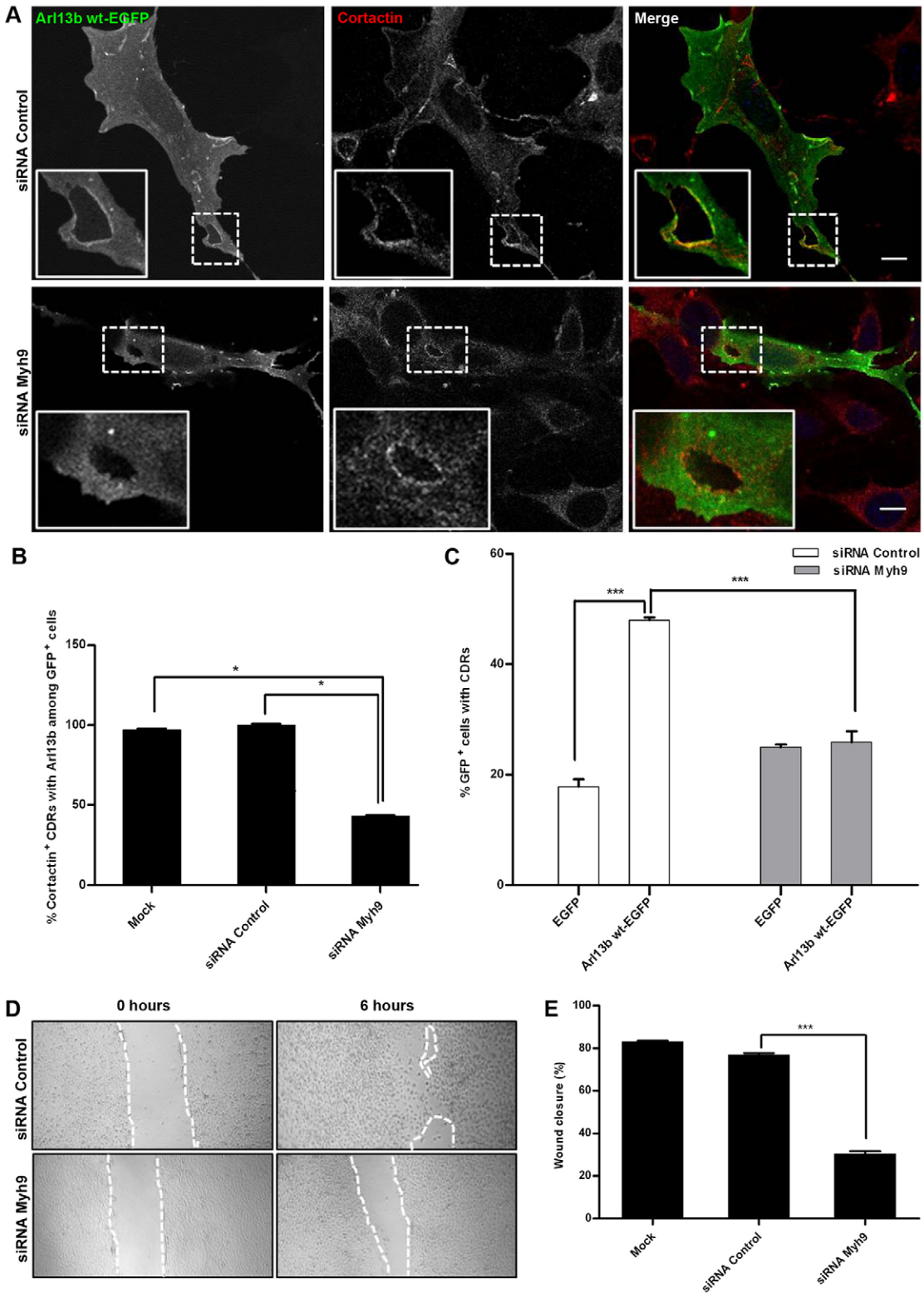

Fig. 7. See next page for legend.

(GAPs), such as ASAP1 and ASAP3, has been shown to strongly inhibit CDR formation (Randazzo et al., 2000). In another study, the Arf GAP ARAP1 has been shown to regulate CDR size through Arf1 and Arf5 (Hasegawa et al., 2012). However, to our knowledge, Arl13b is the first Arl reported to date to localize to CDRs and to regulate their formation. Furthermore, CDRs have been associated with cell migration (Hoon et al., 2012). Supporting an important function for Arl13b in the formation and function of these structures, we have shown that cells silenced for Arl13b are defective in CDR formation and cell migration. Conversely, overexpression of Arl13b promotes CDR formation and cell motility. Importantly, we have also shown that

Journal of Cell Science (2014) 127, 2709–2722 doi:10.1242/jcs.143446

Fig. 7. Myh9 is necessary for Arl13b-mediated CDR formation and cell migration. NIH-3T3 cells silenced for Myh9 and control cells (mock and siRNA Control) were transfected with Arl13b–wt-EGFP (Arl13b wt-EGFP) or EGFP, serum-starved and stimulated with PDGF-BB (30 ng/ml) for 10 minutes. Cells were fixed and stained with anti-cortactin antibody to identify CDRs. (A) Immunofluorescence analysis of CDRs after transfection of Myh9-silenced or control cells with Arl13b-wt–EGFP. Enlarged views of the indicated sections are shown in the insets. Scale bars: 10 μm. (B) Quantification of cortactin-positive CDRs containing Arl13b-wt–EGFP. Results are mean±s.d. of three independent experiments; >150 cells counted per experiment in each condition. (C) After transfection of EGFP or Arl13b-wt–EGFP in Myh9-silenced or control cells, the number of EGFP-positive cells containing at least one CDR after PDGF stimulation was counted. Results are mean±s.d. of three independent experiments; >100 cells counted per condition). (D) Myh9-silenced and control cells grown to confluence were serum-starved and the monolayer was scratched using a pipette tip. Wound closure was monitored for 6 hours. Representative images for both control siRNA and siRNA for Myh9 are shown. (E) The wound area was measured at 0 and 6 hours. Wound closure (%), quantified as described in Materials and Methods was determined in three independent experiments. *$P<0.05$ (B, Student's *t*-test); ***$P<0.001$ (C,E; two-way ANOVA).

PDGF-stimulated cell migration is accompanied by an increase in the formation of Arl13b-positive CDRs in migrating cells. These findings suggest that Arl13b is involved in growth-factor-induced actin remodeling and provide insights into the molecular mechanism by which Arl13b is necessary for cell migration. Interestingly, it has recently been shown that Arl13b in primary cilia is required for efficient interneuronal migration into the dorsal cerebral cortex (Higginbotham et al., 2012). In particular, those authors observed that Arl13b is required for ciliary localization of receptors for interneuronal migration guidance cues, such as 5-hydroxytryptamine (serotonin) receptor subtype 6 (5-HTR6). In this study, we have shown that HeLa cells, which lack primary cilia, display impaired cell migration when Arl13b is silenced. This suggests that the role of Arl13b in cell migration is more general and independent of cilia. Moreover, we monitored the migration of neural crest cells *in vivo* in a vertebrate model organism, the zebrafish. Whether cilia are present in trunk neural crest is not yet fully clear. Nevertheless, this experiment confirmed that Arl13b deficiency reduces the migration of neural crest cells, a defect that could be rescued by the exogenous expression of the protein in Arl13b transgenic zebrafish.

Small G proteins can bind various effectors, such as motors, kinases and phosphatases, in their GTP-bound active conformation. Herein, we have identified a new Arl13b effector, the non-muscle myosin heavy chain IIA, also known as Myh9, which interacts with Arl13b only in its GTP-bound form. To our knowledge, Myh9 is the first bona fide Arl13b effector found to date. Myh9 is one of three distinct isoforms of the non-muscle myosin II heavy chain, an actin-dependent motor protein involved in the regulation of cell adhesion, cell migration and tissue architecture (Vicente-Manzanares et al., 2009). Previous studies have shown that Myh9 depletion by siRNA results in defects in cell migration and lamellar spreading (Betapudi et al., 2006). Moreover, Myh9 has been shown to be required for internalization of EGF (Kim et al., 2012). We found that Myh9 and Arl13b colocalize in PDGF-induced CDRs and that silencing of Myh9 expression by siRNA impairs CDR formation. Similar to what has been described by others, we confirmed that Myh9 silencing impairs cell migration. We have also found that the interaction between Arl13b and actin requires Myh9. However, it remains to be established whether the Myh9 interaction with Arl13b is direct and, if so, what is (are) the domain(s) involved in the interaction.

Cell migration hinges on trafficking of signaling and adhesion molecules towards the leading edge, a process that requires the regulation of cytoskeletal and vesicle trafficking machineries. Impairment of the endocytic and/or exocytic trafficking of integrins dramatically affects the polarity and directionality of cell migration (Caswell and Norman, 2008). In addition, it has been shown that CDRs recruit cell surface integrins and internalize them through macropinocytosis for recycling towards the leading edge of migrating cells (Gu et al., 2011). Given that we have shown that Arl13b regulates endocytic recycling traffic (Barral et al., 2012) and found that, upon PDGF stimulation, Arl13b associates with macropinosomes and with early and recycling endosomes, it is plausible that Arl13b is involved in integrin recycling towards the leading edge in growth-factor-stimulated cell migration. However, this remains to be established.

Thus, our results uncover an important function for Arl13b in processes that are dependent on actin cytoskeleton remodeling and culminate with cell migration, and suggest that the interaction between Arl13b and Myh9 is necessary for the generation of contractile forces that are required for this process.

MATERIALS AND METHODS

Cell culture

Cell culture reagents were obtained from Invitrogen. HeLa cells were maintained at 37°C and 5% CO_2, in Dulbecco's modified Eagle's medium (DMEM, Invitrogen) supplemented with 10% fetal bovine serum (FBS, Invitrogen), 100 U/ml penicillin G, 100 μg/ml streptomycin, 2 mM L-glutamine and 20 mM HEPES (Invitrogen). NIH-3T3 cells were maintained in the same medium with 10% bovine calf serum (Sigma), instead of FBS. Wild-type and *Arl13b*^{hnn} immortalized mouse embryonic fibroblasts (MEFs, a kind gift of Tamara Caspary, Department of Human Genetics, Emory University, Atlanta, GA) were maintained in dishes coated with 0.2% gelatin (Sigma) in the same medium as HeLa cells, further supplemented with 1 g/l sodium bicarbonate. Primary human fibroblasts were established from skin biopsies and grown in the same medium as HeLa cells with 5% FBS (Invitrogen). To stimulate CDR formation and cell migration, cells were serum-starved for the indicated periods, followed by PDGF-BB (Sigma) addition at a final concentration of 20–30 ng/ml for the indicated periods, before being analyzed.

Transfection and constructs

Transfections were performed using Lipofectamine 2000 (Invitrogen) according to the manufacturer's instructions and experiments performed 24 hours after transfection. Arl13b-wt–EGFP construct was a kind gift from Kenji Kontani (University of Tokyo, Japan). Arl13b-1–193–EGFP mutant was as described previously (Barral et al., 2012). Lifeact-ruby plasmid was obtained from Abp140-17aaRuby-nos1-3′UTR (B007) (modified by R. Mateus, CEDOC, Riedl et al., 2008). Rab5a was amplified by PCR using primers 5′-CAGCGAATTCATGGCTAATCGAGGAGCAACAAGAC-CCAAC-3′ (forward) and 5′-ACACGTCGACGGAATAGCCAACA-TGA-3′, and then cloned into pcDNA ENTRBPV5 mcherry-C2 using *Eco*RI/*Sal*I. pcDNA ENTR BP V5 mcherry-C2 was constructed on a backbone of pcDNA6.2/GW/EmGFP (Invitrogen), an expression mammalian vector with Gateway technology (Invitrogen), by swapping EmGFP by V5 and polylinker, using *Dra*I. mCherry was amplified from pCMV myc-mCherry, using 5′-GATCAGATCTATGGTGAGCAAG-GGCGAGGAGGATAAC-3′ (forward) and 5′-TCGAGTCCTTGTACA-GCTCGTCCATGCGCCG-3′ (reverse) as primers, and then cloned using *Bgl*II/*Xho*I. siRNA smart pool against Myh9 and siRNA genome non-targeting sequence no. 3, used as control, were transfected with Dharmafect 1 reagent (Dharmacon), according to the manufacturer's instructions. Experiments were performed after 72–96 hours of transfection with siRNAs.

Cell transduction

NIH-3T3, HeLa or primary human fibroblasts were plated at 2×10^5 cells per well on six-well plates and infected with shRNA-encoding lentiviruses the next day. For this, 6 μg/ml polybrene (hexadimethrine bromide, Sigma) was added to the cells before the virus. After 24 hours, 2 μg/ml puromycin (Sigma) was added and cells selected for at least a

week before being assayed. The shRNA sequences for human cells and the negative control sequence (Mission) are described elsewhere (Barral et al., 2012). For mouse cells, the shRNA sequences are: F2, 5′-CGGCCTTGATAATGCTGGTAA-3′; F3, 5′-GCAAAGGACTTTG-ATGCCTTA-3′; and F5, 5′-CCTGTCAGAAAGGTGACACTT-3′. Primary human fibroblasts grown on coverglasses placed inside 24-well plates (1×10^4 cells per well) were infected with L13 Arl13b-EGFP lentivirus (a kind gift from Tamara Caspary) in the presence of 6 µg/ml polybrene for 5 days. Cells were then serum-starved for 5 hours in DMEM supplemented with 0.5% BSA, and CDR formation was stimulated by the addition of PDGF-BB (20 ng/ml, Sigma).

Immunoblotting and immunoprecipitation

Cells were lysed in cold lysis buffer (50 mM Tris-HCl pH 7.4, 0.1% Triton X-100, 150 mM NaCl, 1 mM EDTA, 1 mM EGTA, 2 mM $MgCl_2$ and 1 mM DTT), in the presence of protease and phosphatase inhibitors, for 30 minutes on ice, followed by centrifugation at 12,000 ***g*** for 15 minutes at 4℃. Protein concentration was determined using the DC protein assay kit (Bio-Rad) and equal amounts (50 µg) of each sample were loaded on 8–10% SDS-polyacrilamide gels, transferred onto nitrocellulose membranes in transfer buffer (25 mM Tris, 192 mM glycine, 0.025% SDS and 20% methanol) for 90 minutes at 500 mA and processed for immunoblotting. Membranes were blocked with blocking buffer (5% skimmed milk and 0.1% Tween-20 in PBS) and the antibodies incubated in the same buffer. Affinity-purified rabbit polyclonal anti-Arl13b antibody (Barral et al., 2012) was used at 3 µg/ml, anti-GAPDH antibody (SicGen) at 0.2 µg/ml, anti-Myh9 antibody (Sigma) at 1 µg/ml. Horseradish peroxidase (HRP)-conjugated secondary antibodies (GE Healthcare) were used at 0.4 µg/ml. Blots were developed with the Immun-Star™ WesternC™ chemiluminescent kit (Bio-Rad) according to the manufacturer's instructions and a Molecular Imager Chemidoc XRS (Bio-Rad) was used to detect the chemiluminescence. Band intensities were quantified using ImageJ software and normalized using GAPDH as a loading control. For immunoprecipitation, cell lysates (1.5 mg total protein) were pre-cleared for 1 hour with Protein-G–Sepharose beads (Sigma). GTPγS (0.5 mM, Sigma) or GDP (5 mM, Sigma) were added to the pre-cleared lysates for 15 minutes at room temperature. Immunoprecipitation was performed using anti-β-actin (Sigma, clone AC-15, 1 µg/ml) or affinity purified rabbit polyclonal anti-Arl13b antibody (3 µg/ml; Barral et al., 2012) for 16 hours at 4℃ with rotation. Protein-G–Sepharose beads were then added and mixed for 4 hours at 4℃. Beads were recovered by centrifugation, washed once with lysis buffer with a high salt concentration (500 mM NaCl), three times with lysis buffer, and finally were resuspended in Laemmli sample buffer. After boiling at 95℃ for 5 minutes, the immunoprecipitates were resolved by 8–10% SDS-PAGE followed by immunoblotting with anti-Myh9 or anti-Arl13b antibodies or visualization with Colloidal Coomassie BB (Neuhoff et al., 1988).

Dextran and transferrin internalization assay

To analyze macropinocytosis, NIH-3T3 cells were transfected with Arl13b-wt–EGFP for 24 hours, serum-starved for 5 hours and further stimulated with PDGF-BB (25 ng/ml) together with 0.3 mg/ml tetramethylrhodamine-labeled lysine-fixable 10 kDa dextran (Invitrogen) in serum-free DMEM for 5, 10 or 20 minutes at 37℃. The cells were washed three times with pre-chilled PBS, fixed with 4% paraformaldeyde overnight and then stained with Alexa-Fluor-568-conjugated phalloidin (Invitrogen). The analysis was performed using a Zeiss 710 LSM confocal microscope equipped with a Plan-Apochromat 63× 1.40 NA oil Ph3 lens and Zeiss Zen 2010 software. For transferrin recycling, NIH-3T3 cells were transfected with Arl13b-wt–EGFP for 24 hours and serum-starved for at least 1 hour and then incubated with PDGF-BB (25 ng/ml) and Alexa-Fluor-546-conjugated transferrin (10 µg/ml, Invitrogen) for 30 minutes at 37℃. The cells were then rinsed in PBS and fixed immediately.

Transwell migration and scratch wound healing assays

Transwell migration assays were performed using modified Boyden chambers. The underside of the polycarbonate membrane (8-µm pore size; Corning) was coated for 16 hours at 4℃ with 10 µg/ml fibronectin (Sigma), washed once with PBS and the chamber filled with DMEM containing 0.5% BSA (starvation medium), with the coated surface facing downward. Cells silenced for Arl13b with shRNAs (F2, F3 and F5) were serum-starved for 5 hours, counted and 1×10^5 cells (in 100 µl) added to the upper chamber compartment for each condition. After 2 hours of incubation at 37℃ and 5% CO_2, 30 ng/ml of PDGF-BB were added into the lower well to induce cell migration. After 6 hours of migration, the upper filter membrane surface was wiped to remove cells that had not migrated through the filter, and the filter was fixed and stained with 0.1% (w/v) Crystal Violet in 20% methanol for 15 minutes to identify cells on the lower filter membrane surface. The number of cells that migrated through the 0.8-mm^2 transwell membrane was counted in at least ten randomly-selected areas in triplicate for each condition and represented as the percentage of migration relative to control cells. For scratch wound healing assays, NIH-3T3, HeLa, *Arl13b*^{hnn} or wild-type MEFs were grown to confluence and the monolayer scratched using 200 µl pipette plastic tips. After washing once with PBS, DMEM supplemented with 0.5% BSA was added together with PDGF-BB (30 ng/ml). Images were taken from each well immediately [time (*t*) 0] and after 8–16 hours. The area of cell migration from the initial wound edge was measured in ten random areas using Zeiss Axiovision software. Wound closure (%) was determined as follows: [1−(wound area at *t*=8–16 hours/wound area at *t*=0 hours)×100]. For immunofluorescence analyses, slides were fixed in 4% paraformaldeyde for 15 minutes at room temperature and further processed for immunofluorescence, using Alexa-Fluor-568-conjugated phalloidin (0.2 units/ml, Invitrogen), anti-cortactin antibody (0.6 mg/ml, Millipore) and DAPI (1 µg/ml, Sigma), to stain nuclei.

Mass spectrometry

For mass spectrometry (MS), immunoprecipitated bands of interest were excised and digested with 6.7 ng/µl trypsin (Promega) in 50 mM NH_4HCO_3 and incubated overnight at 37℃. Digested peptides were desalted and concentrated with microcolumns produced in-house using GELoader tips packed with POROS R2 (Applied Biosystems, 20-µm bead size) and eluted directly onto the matrix-assisted laser desorption/ionization (MALDI) plate using 0.6 µl of 5 mg/ml a-CHCA (a-cyano-4-hydroxy-trans-cinnamic acid, Sigma) in 50% (v/v) acetonitrile (ACN) with 5% (v/v) formic acid and allowed to air dry. MS and tandem MS (MS/MS) spectra were acquired using 4800 plus MALDI-time-of-flight (TOF)/TOF and using 4000 Series Explorer Software v.3.5.3 (Applied Biosystems). The mass spectrometer was externally calibrated using a standard peptide mixture containing angiotensin II (1046.2 Da), angiotensin I (1296.5 Da), neurotensin (1672.9 Da), ACTH (1–17; 2093.5 Da) and ACTH (18–39; 2465.7 Da) (LaserBio Labs). Each MS spectrum was acquired in a result-independent acquisition mode and the 10–15 strongest precursors were selected for MS/MS analyses. These were performed using collision-induced dissociation (CID) assisted with atmospheric air with acollision energy of 1 kV and a gas pressure of 1×10^6 Torr. The MS and MS/MS data was analyzed in combined search mode (MS+MS/MS) using GPS Explorer Software v. 3.6 (Applied Biosystems) and the MASCOT search engine. The search parameters were as follows: monoisotopic peptide mass values were considered, maximum precursor mass tolerance (MS) of 50 ppm and a maximum fragment mass tolerance (MS/MS) of 0.3 Da. A maximum of two missed cleavages were allowed and no taxonomy restrictions were included. Carboxyamidomethylation of cysteines and oxidation of methionines were set as variable modifications. Protein identification was considered by use of significant homology scores if $P<0.05$ and if at least one peptide was fragmented.

Immunofluorescence

Cells grown on glass coverslips were serum-starved for 5 to 16 hours, stimulated or not with PDGF (30 ng/ml) for different times, washed with PBS and fixed in 4% paraformaldehyde in PBS for 15–20 minutes at room temperature. After quenching with 50 mM NH_4Cl in PBS and blocking and permeabilizing with PBS, 0.5% BSA and 0.1% saponin for 10 minutes at room temperature, anti-Myh9, anti-cortactin, anti-EEA1 antibodies or Alexa-Fluor-568-conjugated phalloidin (0.2 to 0.8 U/ml)

were added in the same buffer for 1 hour at room temperature and the cells were washed five times after each incubation. Secondary Alexa-Fluor-488- or -568-conjugated anti-rabbit or anti-mouse antibodies (Invitrogen) were used at 2–4 µg/ml. Coverslips were mounted in mounting medium [15% (w/v) vinol 205, 33% (v/v) glycerol, 0.1% azide in PBS] and analyzed in a Zeiss LSM 710 confocal microscope equipped with a Plan-Apochromat 63× 1.40 NA oil Ph3 lens and Zeiss Zen 2010 software or a Leica TCS SP5 confocal microscope equipped with a HCX PL-APO 63× (NA 1.25–0.75) lens and Leica Application Suite software. Images were processed with ImageJ software, adjusting the levels or brightness of each channel up to a maximum threshold defined by the absence of signal in the negative controls.

Time-lapse fluorescence microscopy

NIH-3T3 cells were grown in the eight-well Lab-Tek chambered #1.0 borosilicate coverglass system (Thermo Fisher) and transfected with Lifeact-ruby and Arl13b-wt–EGFP constructs using Lipofectamine 2000 (Invitrogen) according to the manufacturer's instructions. After 24 hours, cells were serum-starved in DMEM without Phenol Red and supplemented with 0.5% BSA for 2 hours, and then imaged in the same medium before and after the addition of PDGF-BB (20 ng/ml). The images were acquired for 30 minutes at 60-second intervals by using an Andor Revolution XD system in a Nikon eclipse TiE spinning disk laser confocal microscope, equipped with a sensitive EMCCD camera and Plan Apo VC 60× 1.4 NA objective at 37℃ and under 5% CO_2.

Zebrafish *in situ* hybridization

Zebrafish embryos were obtained through natural crosses and staged according to Kimmel et al. (Kimmel et al., 1995). The Arl13b morpholino was as described previously (Duldulao et al., 2009). Embryos were injected at the one-cell stage, fixed at 24 hours post-fertilization and hybridized with a *sox10* probe. Whole-mount *in situ* hybridization was performed as described previously (Thisse and Thisse, 2008). Dioxigenin RNA probe was synthesized from a *sox10* DNA template kindly provided by Robert N. Kelsh (University of Bath, UK; Dutton et al., 2001). All animal experiments were performed according to approved guidelines.

Statistical analysis

Numerical data are presented as mean±s.d. Statistical analysis was performed using GraphPad Prism (version 5.00, GraphPad Software). Two-way ANOVA or Student's *t*-tests were used for comparison between different data sets by using GraphPad Prism software.

Acknowledgements

We thank Tamara Caspary (Emory University, Atlanta, GA), Kenji Kontani (University of Tokyo) and Robert Kelsh (University of Bath, UK) for the kind gift of reagents. We thank Lúcia Lacerda (Instituto Nacional de Saúde Dr. Ricardo Jorge, Portugal) for kindly providing primary human fibroblasts. We also thank Ana Varela Coelho, from the Mass Spectrometry Laboratory, Analytical Services Unit (Instituto de Tecnologia Química e Biológica, Universidade Nova de Lisboa, Portugal).

Competing interests

The authors declare no competing interests.

Author contributions

C.C. performed most of the experiments. C.S. performed the mass spectrometry identification experiments together with M.B. Dextran internalization experiments were performed by A.P. J.R. made the Rab5–mCherry construct. Experiments using zebrafish were performed by P.P. under the supervision of S.L. The manuscript was written by C.C. and D.C.B. The study was supervised by D.C.B.

Funding

This work was supported by a Marie Curie International Reintegration Grant [grant number Marie Curie_PIRG05-GA-2009-247726 to D.C.B.]; by postdoctoral fellowships from Fundação para a Ciência e Tecnologia (FCT) [grant numbers SFRH/BPD/78561/2011 to C.C., SFRH/BPD/32323/2006 to C.S.]; a PhD fellowship from FCT [grant number SFRH/BD/68502/2010 to A.P.]; and a FCT grant [grant number PTDC/SAU-OBD/103981/2008 to S.L.].

Supplementary material

Supplementary material available online at
http://jcs.biologists.org/lookup/suppl/doi:10.1242/jcs.143446/-/DC1

References

Alieva, I. B., Gorgidze, L. A., Komarova, Y. A., Chernobelskaya, O. A. and Vorobjev, I. A. (1999). Experimental model for studying the primary cilia in tissue culture cells. *Membr. Cell Biol.* **12**, 895-905.

Ammer, A. G. and Weed, S. A. (2008). Cortactin branches out: roles in regulating protrusive actin dynamics. *Cell Motil. Cytoskeleton* **65**, 687-707.

Barral, D. C., Garg, S., Casalou, C., Watts, G. F. M., Sandoval, J. L., Ramalho, J. S., Hsu, V. W. and Brenner, M. B. (2012). Arl13b regulates endocytic recycling traffic. *Proc. Natl. Acad. Sci. USA* **109**, 21354-21359.

Betapudi, V., Licate, L. S. and Egelhoff, T. T. (2006). Distinct roles of nonmuscle myosin II isoforms in the regulation of MDA-MB-231 breast cancer cell spreading and migration. *Cancer Res.* **66**, 4725-4733.

Bond, L. M., Brandstaetter, H., Sellers, J. R., Kendrick-Jones, J. and Buss, F. (2011). Myosin motor proteins are involved in the final stages of the secretory pathways. *Biochem. Soc. Trans.* **39**, 1115-1119.

Borovina, A., Superina, S., Voskas, D. and Ciruna, B. (2010). Vangl2 directs the posterior tilting and asymmetric localization of motile primary cilia. *Nat. Cell Biol.* **12**, 407-412.

Buccione, R., Orth, J. D. and McNiven, M. A. (2004). Foot and mouth: podosomes, invadopodia and circular dorsal ruffles. *Nat. Rev. Mol. Cell Biol.* **5**, 647-657.

Cantagrel, V., Silhavy, J. L., Bielas, S. L., Swistun, D., Marsh, S. E., Bertrand, J. Y., Audollent, S., Attié-Bitach, T., Holden, K. R., Dobyns, W. B. et al.; **International Joubert Syndrome Related Disorders Study Group** (2008). Mutations in the cilia gene ARL13B lead to the classical form of Joubert syndrome. *Am. J. Hum. Genet.* **83**, 170-179.

Caspary, T., Larkins, C. E. and Anderson, K. V. (2007). The graded response to Sonic Hedgehog depends on cilia architecture. *Dev. Cell* **12**, 767-778.

Caswell, P. and Norman, J. (2008). Endocytic transport of integrins during cell migration and invasion. *Trends Cell Biol.* **18**, 257-263.

Conti, M. A. and Adelstein, R. S. (2008). Nonmuscle myosin II moves in new directions. *J. Cell Sci.* **121**, 11-18.

Donaldson, J. G. and Jackson, C. L. (2011). ARF family G proteins and their regulators: roles in membrane transport, development and disease. *Nat. Rev. Mol. Cell Biol.* **12**, 362-375.

Dowrick, P., Kenworthy, P., McCann, B. and Warn, R. (1993). Circular ruffle formation and closure lead to macropinocytosis in hepatocyte growth factor/scatter factor-treated cells. *Eur. J. Cell Biol.* **61**, 44-53.

Duldulao, N. A., Lee, S. and Sun, Z. (2009). Cilia localization is essential for in vivo functions of the Joubert syndrome protein Arl13b/Scorpion. *Development* **136**, 4033-4042.

Dutton, K. A., Pauliny, A., Lopes, S. S., Elworthy, S., Carney, T. J., Rauch, J., Geisler, R., Haffter, P. and Kelsh, R. N. (2001). Zebrafish colourless encodes sox10 and specifies non-ectomesenchymal neural crest fates. *Development* **128**, 4113-4125.

Even-Ram, S., Doyle, A. D., Conti, M. A., Matsumoto, K., Adelstein, R. S. and Yamada, K. M. (2007). Myosin IIA regulates cell motility and actomyosin-microtubule crosstalk. *Nat. Cell Biol.* **9**, 299-309.

Fletcher, S. J. and Rappoport, J. Z. (2010). Moving forward: polarised trafficking in cell migration. *Trends Cell Biol.* **20**, 71-78.

Gu, Z., Noss, E. H., Hsu, V. W. and Brenner, M. B. (2011). Integrins traffic rapidly via circular dorsal ruffles and macropinocytosis during stimulated cell migration. *J. Cell Biol.* **193**, 61-70.

Hasegawa, J., Tsujita, K., Takenawa, T. and Itoh, T. (2012). ARAP1 regulates the ring size of circular dorsal ruffles through Arf1 and Arf5. *Mol. Biol. Cell* **23**, 2481-2489.

Higginbotham, H., Eom, T.-Y., Mariani, L. E., Bachleda, A., Hirt, J., Gukassyan, V., Cusack, C. L., Lai, C., Caspary, T. and Anton, E. S. (2012). Arl13b in primary cilia regulates the migration and placement of interneurons in the developing cerebral cortex. *Dev. Cell* **23**, 925-938.

Hoon, J.-L., Wong, W.-K. and Koh, C.-G. (2012). Functions and regulation of circular dorsal ruffles. *Mol. Cell. Biol.* **32**, 4246-4257.

Horner, V. L. and Caspary, T. (2011). Disrupted dorsal neural tube BMP signaling in the cilia mutant Arl13b hnn stems from abnormal Shh signaling. *Dev. Biol.* **355**, 43-54.

Kerr, M. C. and Teasdale, R. D. (2009). Defining macropinocytosis. *Traffic* **10**, 364-371.

Kim, J. H., Wang, A., Conti, M. A. and Adelstein, R. S. (2012). Nonmuscle myosin II is required for internalization of the epidermal growth factor receptor and modulation of downstream signaling. *J. Biol. Chem.* **287**, 27345-27358.

Kimmel, C. B., Ballard, W. W., Kimmel, S. R., Ullmann, B. and Schilling, T. F. (1995). Stages of embryonic development of the zebrafish. *Dev. Dyn.* **203**, 253–310.

Lanzetti, L., Palamidessi, A., Areces, L., Scita, G. and Di Fiore, P. P. (2004). Rab5 is a signalling GTPase involved in actin remodelling by receptor tyrosine kinases. *Nature* **429**, 309-314.

Larkins, C. E., Aviles, G. D. G., East, M. P., Kahn, R. A. and Caspary, T. (2011). Arl13b regulates ciliogenesis and the dynamic localization of Shh signaling proteins. *Mol. Biol. Cell* **22**, 4694-4703.

Neuhoff, V., Arold, N., Taube, D. and Ehrhardt, W. (1988). Improved staining of proteins in polyacrylamide gels including isoelectric focusing gels with clear background at nanogram sensitivity using Coomassie Brilliant Blue G-250 and R-250. *Electrophoresis* **9**, 255-262.

Orth, J. D. and McNiven, M. A. (2006). Get off my back! Rapid receptor internalization through circular dorsal ruffles. *Cancer Res.* **66**, 11094-11096.

Palamidessi, A., Frittoli, E., Garré, M., Faretta, M., Mione, M., Testa, I., Diaspro, A., Lanzetti, L., Scita, G. and Di Fiore, P. P. (2008). Endocytic trafficking of Rac is required for the spatial restriction of signaling in cell migration. *Cell* **134**, 135-147.

Raftopoulou, M. and Hall, A. (2004). Cell migration: Rho GTPases lead the way. *Dev. Biol.* **265**, 23-32.

Randazzo, P. A., Nie, Z., Miura, K. and Hsu, V. W. (2000). Molecular aspects of the cellular activities of ADP-ribosylation factors. *Sci. STKE* **2000**, re1.

Ridley, A. J., Schwartz, M. A., Burridge, K., Firtel, R. A., Ginsberg, M. H., Borisy, G., Parsons, J. T. and Horwitz, A. R. (2003). Cell migration: integrating signals from front to back. *Science (New York, N.Y.)* **302**, 1704-1709.

Riedl, J., Crevenna, A. H., Kessenbrock, K., Yu, J. H., Neukirchen, D., Bista, M., Bradke, F., Jenne, D., Holak, T. A., Werb, Z. et al. (2008). Lifeact: a versatile marker to visualize F-actin. *Nat. Methods* **5**, 605-607.

Sero, J. E., Thodeti, C. K., Mammoto, A., Bakal, C., Thomas, S. and Ingber, D. E. (2011). Paxillin mediates sensing of physical cues and regulates directional cell motility by controlling lamellipodia positioning. *PLoS ONE* **6**, e28303.

Swanson, J. A. (2008). Shaping cups into phagosomes and macropinosomes. *Nat. Rev. Mol. Cell Biol.* **9**, 639-649.

Thisse, C. and Thisse, B. (2008). High-resolution in situ hybridization to whole-mount zebrafish embryos. *Nat. Protoc.* **3**, 59-69.

Ulrich, F. and Heisenberg, C.-P. (2009). Trafficking and cell migration. *Traffic* **10**, 811-818.

Vicente-Manzanares, M., Ma, X., Adelstein, R. S. and Horwitz, A. R. (2009). Non-muscle myosin II takes centre stage in cell adhesion and migration. *Nat. Rev. Mol. Cell Biol.* **10**, 778-790.

Journal of Cell Science

Supplementary Figure S1 - Localization of Arl13b in CDRs of human and mouse fibroblasts. (A) Normal human primary fibroblasts were transduced with L13 Arl13b-wt-EGFP (Arl13b wt-EGFP) lentiviruses, serum-starved for 16 hours and stimulated with PDGF-BB (30 ng/ml) for the indicated times. Cells were then fixed and stained with Alexa-Fluor-568-conjugated phalloidin or with mouse monoclonal anti-cortactin antibody followed by anti-mouse secondary Alexa-Fluor-488-conjugated antibody. Scale bars: 10 μm. **(B)** NIH-3T3 cells transiently transfected with Arl13b-wt-EGFP and Lifeact-ruby were serum-starved, stimulated with PDGF-BB (20 ng/ml) and processed for live cell imaging. The first 20 minutes of the time-lapse sequence are represented. Arrowheads show a CDR in which Arl13b-wt-EGFP and Lifeact-ruby co-localize. Enlarged views of the indicated sections are shown in the insets. Scale bar: 10 μm.

Supplementary Figure S2 - Arl13b is required for CDR formation in mouse and human fibroblasts (A) NIH-3T3 cells transduced with Arl13b shRNAs (F2 and F3) or control shRNA (Mission), were serum-starved and stimulated with PDGF for 10 minutes (30 ng/ml). Representative immunoblot of three independent experiments showing the expression of Arl13b (top panels) and GAPDH (bottom panels), used as a loading control. Quantification is shown below (AU, arbitrary units). **(B)** *Arl13b*^{hnn} (*hnn*) and wild-type (wt) MEFs were serum-starved for 16 hours and stimulated with PDGF-BB (30 ng/ml) for 30 minutes. After fixation, cells were stained with Alexa-Fluor-568-conjugated phalloidin and mouse monoclonal anti-cortactin antibody, followed by Alexa-Fluor-488-conjugated anti-mouse secondary antibody. Representative images are shown, where DAPI was used to stain nuclei. Arrows indicate CDRs. Scale bar: 10 μm. **(C)** CDR formation in *Arl13b*^{hnn} (*hnn*) and wild-type (wt) MEFs was quantified. Results are mean ± SD of three independent experiments, >200 cells counted for each condition. A representative immunoblot where the expression of Arl13b was analyzed in *Arl13b*^{hnn} (*hnn)* and wild-type (wt) MEFs, with anti-Arl13b antibody (top panel) and anti-GAPDH antibody, as a loading control (bottom panel), is shown below, indicating the percentage of Arl13b expression relative to wild-type (wt). **(D)** CDR formation was quantified in primary human fibroblasts transduced with lentiviruses encoding shRNA for human Arl13b (E3 and E4) or control shRNA (Mission). After stimulation with PDGF-BB for 10 minutes, cells were stained as in (B) and CDRs counted. Results are mean ± SD of three independent experiments,

>160 cells counted per experiment in each condition. A representative immunoblot is shown below, where Arl13b expression was determined using the same antibodies as in (C). The percentage of Arl13b expression relative to control is indicated. ***P<0.001 in (C) and (D), two-way ANOVA.

Supplementary Figure S3 – Role of Arl13b in cell migration of mouse embryonic fibroblasts and HeLa cells. Monolayers of *Arl13b*^{hnn} (*hnn*) and wild-type (wt) MEFs were scratched with a pipette tip and wound closure was monitored for 16 hours. **(A)** Representative images for *Arl13b*^{hnn} (*hnn*) and wild-type (wt) MEFs were taken at time zero and 16 hours post-wounding. **(B)** Quantitative analysis of wound closure (%) after 16 hours was done as described in Materials and Methods. Results are mean ± SD of three independent experiments. **(C)** HeLa cells transduced with viruses encoding shRNAs for human Arl13b (E3 and E4) or control shRNA (Mission) were scratched and wound closure (%) was measured after 10 hours. A representative immunoblot is shown below, where Arl13b expression in Arl13b-silenced or control cells was probed with anti-Arl13b antibody and GAPDH was used as a loading control. The percentage of Arl13b expression relative to control is indicated. **(D)** HeLa cells expressing Arl13b-wt-EGFP (Arl13b wt-EGFP), Arl13b-1-193-EGFP (Arl13b 1-193-EGFP) or EGFP for 24 hours were allowed to form a monolayer and then scratched as described in Materials and Methods. Quantitative analysis of wound closure (%) was performed at 8 hours post-wounding. Results are mean ± SD of three independent experiments). **P<0.005 in (B), (C) and (D), *t*-test.

Supplementary Figure S4 – Arl13b is recruited towards the leading edge of migrating cells and its interaction with β-actin is enhanced by incubation with GTPγS and PDGF stimulation. **(A)** Monolayers of HeLa cells expressing Arl13b-wt-EGFP (Arl13b wt-EGFP) were scratched as described in Materials and Methods and analyzed at 8 hours post-wounding to examine Arl13b-wt-EGFP localization and the actin cystoskeleton, using Alexa-fluor-568-conjugated phalloidin. DAPI was used to stain nuclei. Arrows indicate co-localization of Arl13b-wt-EGFP with phalloidin at the leading edge of migrating cells. Dashed white lines indicate the wound. Scale bar: 10 μm. **(B)** Quantification of Arl13b expression by immunoblotting, after treating NIH-3T3 cells with shRNA control (Mission) or shRNA for Arl13b (F2 and F5), using anti-

Arl13b polyclonal antibody (top panel) and anti-GADPH antibody (bottom panel), used as a load control. **(C)** NIH-3T3 cell lysates stimulated or not with PDGF for 10 minutes were immunoprecipitated with anti-β-actin antibody in the presence of non-hydrolyzable GTPγS or with an excess of GDP. Quantification of the band intensities is shown below. **(D)** Immunoblot analysis of Myh9 expression in Myh9-silenced NIH-3T3 cells, control and mock-transfected cells. Lysates were analyzed using an anti-Myh9 antibody (top panel) or an anti-GAPDH antibody, as a loading control (bottom panel). Quantification of four independent experiments is shown below (AU, arbitrary units). *P<0.05 in (C) and (D), *t*-test.

Supplementary Movie 1- Arl13b co-localization with F-actin in a CDR after PDGF-BB stimulation. NIH-3T3 cells transfected with Arl13b-wt-EGFP and Lifeact-ruby were serum-starved and stimulated with PDGF-BB (20 ng/ml). Live cell images were taken in a spinning disc confocal microscope with frames taken every minute, for 30 minutes.

SUPPLEMENTARY FIGURE S1

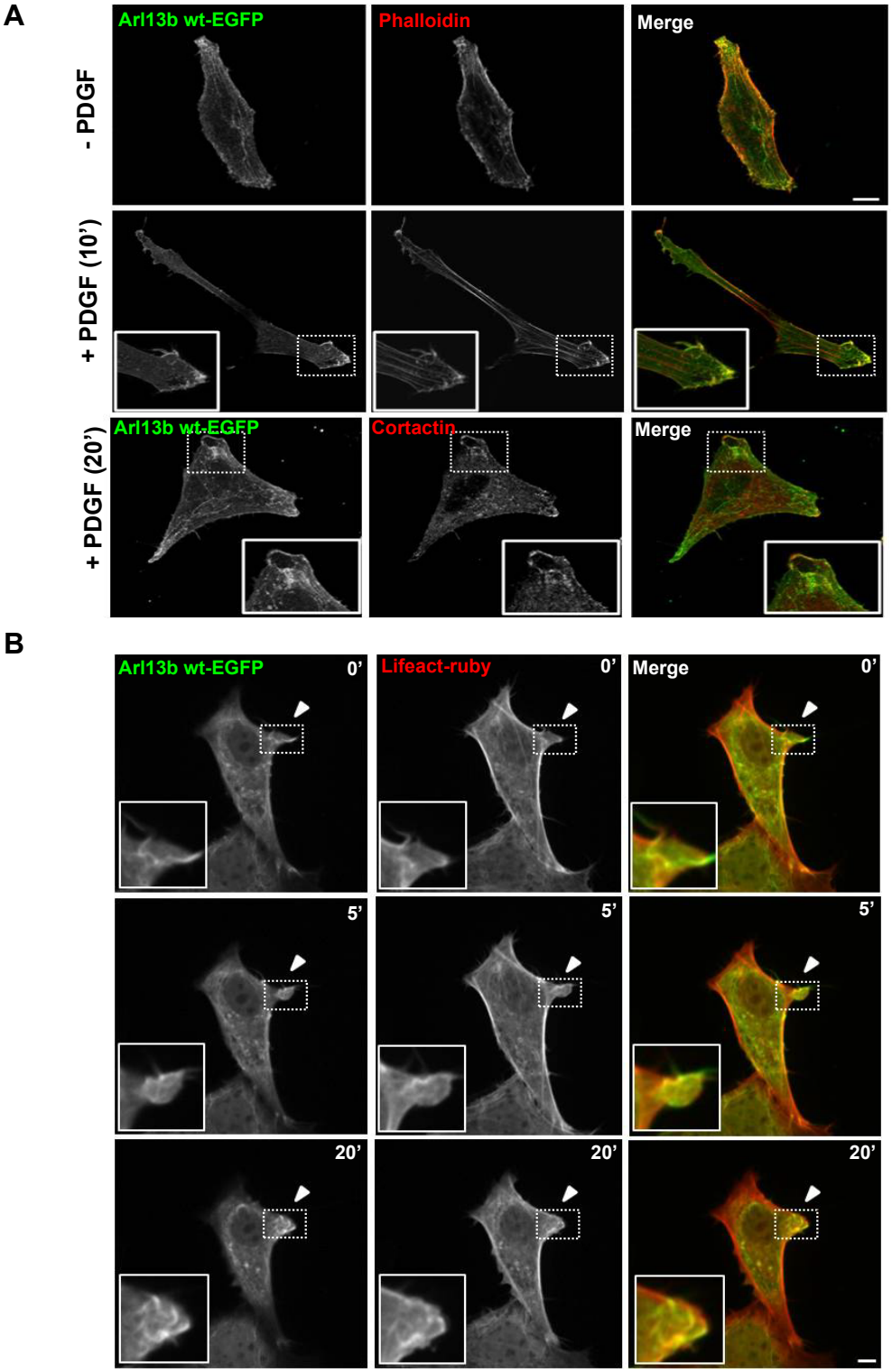

SUPPLEMENTARY FIGURE S2

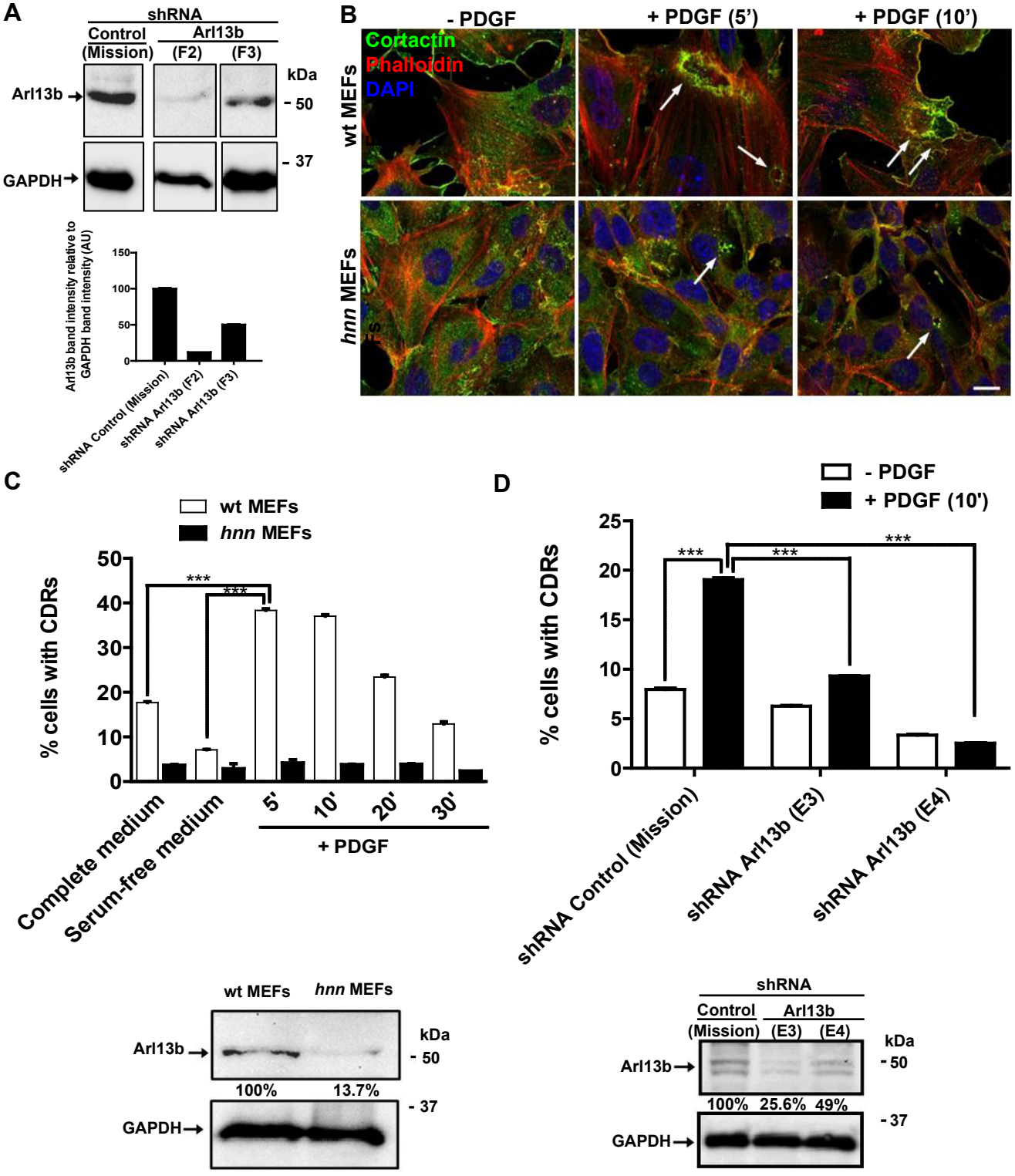

SUPPLEMENTARY FIGURE S3

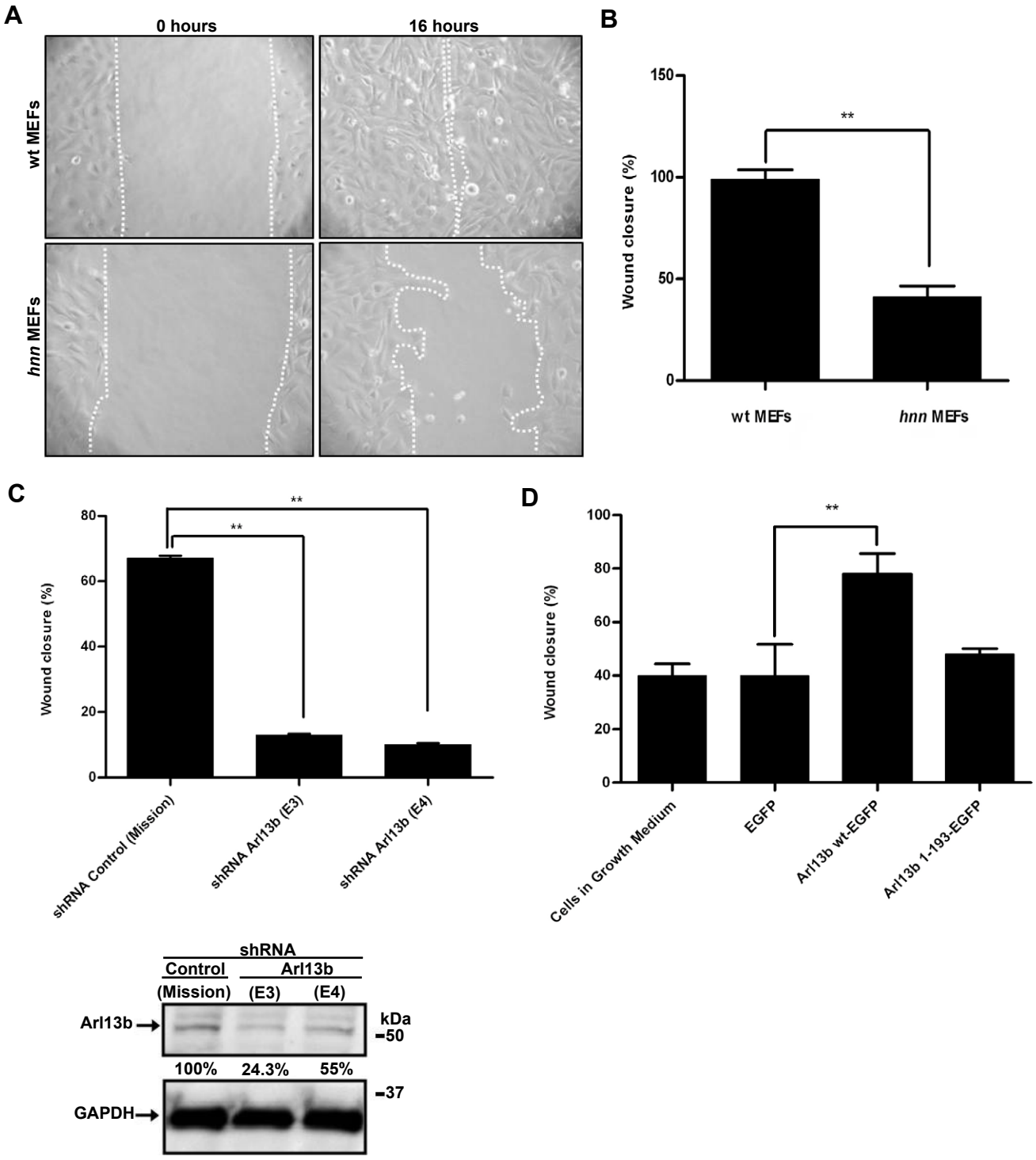

SUPPLEMENTARY FIGURE S4

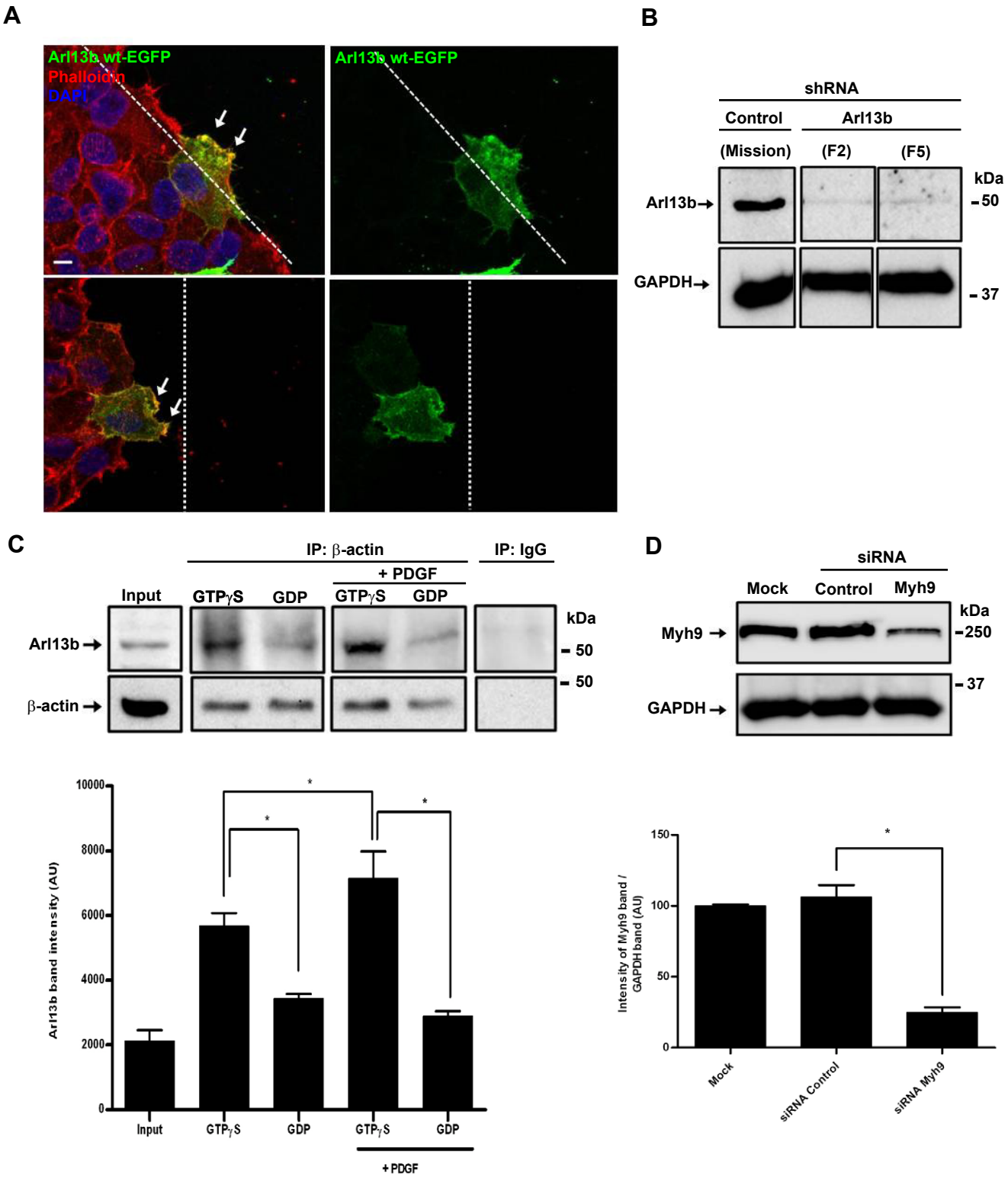

Movie 1.